



Experimental constraints on the physics of cuprates

GUO-MENG ZHAO†

Physik-Institut der Universität Zürich, CH-8057 Zürich, Switzerland

[Received 19 December 2000 and accepted 9 January 2001]

ABSTRACT

Many anomalous physical properties have been observed in the high- T_c cuprate superconductors for the last decade. These include: (1) the unconventional isotope effects on the supercarrier mass, on the charge-stripe formation temperature, on the spin-glass freezing temperature and on the antiferromagnetic ordering temperature; (2) the exotic pairing symmetry shown by many bulk-sensitive experiments; (3) the magnetic resonance peak in the superconducting state revealed by inelastic neutron scattering; (4) the peak, dip and hump features seen in angle-resolved photoemission spectroscopy and in tunnelling spectra; (5) the strong-coupling features in optical and tunnelling data; (6) the pseudogap in the normal state of underdoped cuprates and (7) the unusually large supercarrier mass anisotropy and its novel doping dependence. We review these important experimental results, which can place crucial constraints on the physics of cuprates. The conclusion is that high- T_c superconductivity in cuprates is a cooperative phenomenon between the strong electron–electron correlation and strong electron–phonon coupling.

§1. INTRODUCTION

Developing the microscopic theory for high- T_c superconductivity is one of the most challenging problems in condensed-matter physics. More than 10 years after the discovery of the high- T_c cuprate superconductors by Bednorz and Müller (1986), there have been no microscopic theories that can describe the physics of high- T_c superconductors completely and unambiguously. Owing to the high T_c values and a very small oxygen-isotope effect observed in a 90 K cuprate superconductor $\text{YBa}_2\text{Cu}_3\text{O}_{7-y}$ (YBCO) (Batlogg *et al.* 1987), many theorists believe that the electron–phonon interaction cannot be the origin of high- T_c superconductivity. Most physicists have thus turned their minds towards an alternative pairing interaction of purely electronic origin. In fact, the idea that the highest T_c is only 30 K within the conventional phonon-mediated mechanism is not quite correct. In principle, T_c can increase monotonically with both increasing phonon frequency and increasing electron–phonon coupling constant within the phonon-mediated Eliashberg theory (Carbotte 1990). The limitation of T_c within the phonon mechanism is only imposed by a possible structural instability in the case of too strong an electron–phonon interaction. However, there is no universally accepted, simple and quantitative stability criterion (Carbotte 1990). Therefore, it is quite risky to discard completely the phonon mechanism as the origin of high- T_c superconductivity without looking at

† Email: zhao@physik.unizh.ch

the overwhelming evidence for a strong electron–phonon interaction in these materials. In the same way, it is also dangerous to ignore a strong electron–electron correlation which is crucial to the understanding of the antiferromagnetic (AF) correlation.

In order to develop a correct theory of high- T_c superconductivity, one must understand a generic phase diagram for hole-doped cuprates, as shown in figure 1. For undoped parent compounds, the ground state is AF, suggesting a strong electron–electron correlation. When holes are doped into the CuO_2 planes, the antiferromagnetic state is destroyed rapidly, and superconductivity sets in when the doping level p is above 0.05 per copper atom. The highest T_c is reached at optimal doping with $p_m = 0.15\text{--}0.20$, which separates so-called underdoped ($p < p_m$) and overdoped ($p > p_m$) regimes. In the overdoped range, the superconducting transition appears to be conventional mean-field like, that is the pairing and superconducting condensation occur at the same temperature T_c . The most unusual and striking features observed in cuprates can be summarized as follows.

- (a) T_c is approximately proportional to n_s/m_{ab}^{**} in the deeply underdoped region (where n_s is the supercarrier density and m_{ab}^{**} is the in-plane supercarrier mass).
- (b) The pseudogap is formed above T_c in the underdoped region.
- (c) The supercarrier mass anisotropy $\gamma = (m_c^{**}/m_{ab}^{**})^{1/2}$ increases rapidly with decreasing doping and can reach a value of more than 100.
- (d) The isotope effect on T_c increases markedly with a decrease in doping, and the isotope exponent can be larger than the Bardeen–Cooper–Schrieffer (BCS) prediction.
- (e) The dynamic or static charge and spin stripes are formed below a characteristic temperature.
- (f) The short-range AF ordering even coexists with superconductivity in the deeply underdoped region.

In addition to these exotic properties, the magnetic resonance peak at the AF wave-vector in the superconducting state has been observed in several double-layer

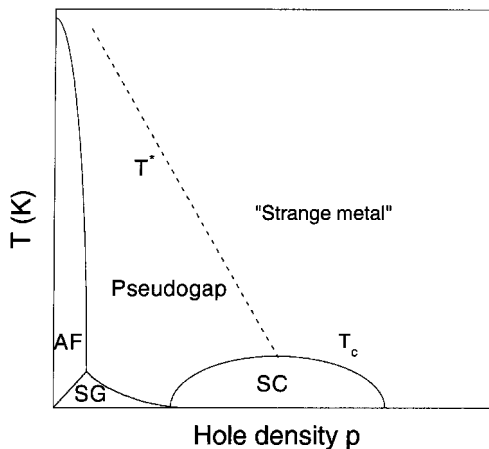


Figure 1. A generic phase diagram for hole-doped cuprates. Here AF, SG and SC represent antiferromagnetic, spin-glass and superconducting ground states respectively.

cuprate systems by inelastic neutron scattering, and an unconventional pairing symmetry has been revealed by many well-designed experiments. The understanding of all these anomalous properties should ultimately lead to a correct microscopic theory of high- T_c superconductivity.

In this review article, we provide quite a number of important and unusual experimental results to place crucial constraints on the basic physics of the high- T_c cuprates. In §2, we present various isotope effects in cuprates including the unconventional isotope effects on the supercarrier mass, on the charge-stripe formation temperature, on the spin-glass freezing temperature and on the AF ordering temperature. These isotope experiments clearly demonstrate that the phonon modes related to both oxygen and copper vibrations are important to the pairing. The results also show that there exist polaronic charge carriers, which are bound into intersite bipolarons in the low-doping regime and into Cooper pairs in the high-doping region. In §3, we identify the intrinsic bulk pairing symmetry for both electron- and hole-doped cuprates from the existing bulk-sensitive and nearly bulk-sensitive experimental results such as the magnetic penetration depth, Raman scattering, single-particle tunnelling, Andreev reflection, nonlinear Meissner effect, neutron scattering and angle-resolved photoemission spectroscopy (ARPES). These experiments consistently show that the dominant bulk pairing symmetry in hole-doped cuprates is of extended s-wave type with eight line nodes, and of anisotropic s-wave type in electron-doped cuprates. The proposed pairing symmetries do not contradict some surface- and phase-sensitive experiments which show a d-wave pairing symmetry at the degraded surfaces. We also quantitatively explain the phase-sensitive experiments along the c axis for both $\text{Bi}_2\text{Sr}_2\text{CaCu}_2\text{O}_{8+y}$ (BSCCO) and YBCO. In §4, we present quantitative explanations for the neutron resonance peak and the spin gap observed in YBCO and BSCCO based on the extended s-wave pairing symmetry in a single-layer CuO_2 plane and opposite signs of the order parameter in the bonding and antibonding electron bands formed within Cu_2O_4 double layers. The neutron resonance peak is due to the excitation of electrons from the bonding band below the superconducting gap to the antibonding band above the superconducting gap. In §5, we shall identify the pairing interaction from neutron, ARPES, tunnelling and optical experiments. These experiments consistently demonstrate that there is a strong interaction between charge carriers and the phonons with energy of about 20 meV. In §6, we provide quantitative explanations for the normal-state susceptibility and propose an electronic structure that is in quantitative agreement with ARPES, optical and transport experiments. We also show that the theory of bipolaronic superconductivity can quantitatively and consistently explain several physical properties such as the doping dependences of the isotope effects, of the supercarrier mass anisotropy, and of the penetration depth in the doping region with $x \leq 0.10$ where nearly all the charge carriers are (bi)polarens. Furthermore, we propose a superconducting mechanism for optimally doped and overdoped cuprates. Finally, we shall give concluding remarks in §7.

§2. UNCONVENTIONAL ISOTOPE EFFECTS

The observation of a gap in the electronic excitation spectrum (Daunt and Mendelssohn 1946) and the discovery of an isotope effect (Maxwell 1950, Reynolds *et al.* 1950) in conventional superconductors provided important and crucial clues to the understanding of the microscopic mechanism of superconductivity. In particular, the effect of changing isotope mass on the super-

conducting transition temperature T_c implies that superconductivity is not of purely electronic origin, but that lattice vibrations (phonons) play an important role in the microscopic mechanism for this phenomenon.

In 1950, the first evidence for an isotope effect was reported by Maxwell (1950) and independently by Reynolds *et al.* (1950). They found that the critical temperature T_c of mercury is an inverse function of the isotope mass. In the same year, Fröhlich (1950) pointed out that the same electron–lattice interaction which describes the scattering of conduction electrons by lattice vibrations gives rise to an indirect interaction between electrons. He proposed that this indirect interaction is responsible for superconductivity. Fröhlich’s theory had strong support from the observed isotope effect and played a decisive role in establishing a correct mechanism. A few years later, Cooper (1956) demonstrated that electrons with an attractive interaction form bound pairs (the so-called Cooper pairs) which lead to superconductivity. However, the existence of electron pairs does not necessarily imply a phonon-mediated pairing. Indeed, Bose condensation as considered by Schafroth (1955) is also a possible mechanism for superconductivity, but the model was not able to explain the isotope effect. Finally, Bardeen *et al.* (1957) developed the BCS theory, which can explain most physical properties observed in conventional superconductors.

Remarkably, the BCS theory can well explain the isotope effect. T_c within the theory is given by (Bardeen *et al.* 1957)

$$k_B T_c = 1.13 \hbar \omega_D \exp\left(-\frac{1}{N(0)V}\right), \quad (1)$$

where ω_D is the Debye frequency, which is proportional to $M^{-1/2}$. The electron–phonon coupling $N(0)V$ is the product of an electron–phonon interaction strength V and the electronic density $N(0)$ of states at the Fermi level, both of which are independent of the ion mass M in the harmonic approximation. This formula implies an isotope-mass dependence of T_c , with an isotope-effect exponent $\alpha = -d(\ln T_c)/d(\ln M) = 1/2$. This is in excellent agreement with the reported isotope effects in the non-transition-metal superconductors (e.g. mercury, tin and lead). In fact, the isotope effect was the first justification of the proposed electron–phonon coupling mechanism.

The conventional phonon-mediated superconducting theory is based on the Migdal adiabatic approximation in which the phonon-induced electron self-energy is given correctly to the order of $(m_b/M)^{1/2} \sim 10^{-2}$, where m_b is the bare mass of an electron. Within this approximation, the density $N(0)$ of states at the Fermi level, the electron–phonon coupling constant λ_{ep} and the effective mass of the supercarriers are all independent of the ionic mass M . However, if the interactions between electrons and nuclear ions are strong enough for electrons to form polarons (quasi-particles dressed by lattice distortions), their effective mass m^* will depend on M . This is because the polaron mass $m^* = m_b \exp(A/\omega)$ (Alexandrov and Mott 1995), where A is a constant and ω is a characteristic optical phonon frequency which depends on the masses of ions. Hence, there is a large isotope effect on the carrier mass in polaronic metals, in contrast with the zero isotope effect in ordinary metals. The total exponent of the isotope effect on m^* is defined as $\alpha_{m^*} = \sum -d(\ln m^*)/d(\ln M_i)$ (M_i is the mass of the i th atom in a unit cell). From this definition and the expression for the polaron mass m^* mentioned above, one readily finds that

$$\alpha_{m^*} = -\frac{1}{2} \ln \left(\frac{m^*}{m_b} \right). \quad (2)$$

The above equation implies that there should be a large negative isotope effect on m^* in polaronic metals.

Therefore, if the electron–phonon interaction is strong enough to form polarons and/or bipolarons, one will expect a substantial isotope effect on the effective mass of supercarriers. We shall present various isotope effects in cuprates including the unconventional isotope effects on the supercarrier mass, on the charge-stripe formation temperature, on the spin-glass freezing temperature and on the AF ordering temperature. These isotope experiments clearly demonstrate that the phonon modes related to both oxygen and copper vibrations are important to the pairing. The results also show that there exist polaronic charge carriers, which are bound into intersite bipolarons in the low-doping regime and into Cooper pairs in the high-doping region.

2.1. Isotope effect on the superconducting transition temperature

Studies of isotope shifts of T_c have been carried out in almost all known cuprates. A comprehensive review was given by Franck (1994). Most of the studies reported so far concern the oxygen-isotope shift (OIS) of T_c by replacing ^{16}O with ^{18}O , partly because the experimental procedures are simple and reliable. Now it is generally accepted that optimally doped cuprates exhibit a small and positive oxygen-isotope exponent α_O . It is found that α_O for optimally doped cuprates decreases with increasing T_c (Zhao *et al.* 2000a). The small OIS observed in the optimally doped cuprates suggest that phonons might not be important in bringing about high-temperature superconductivity.

However, the doping dependence of the OIS has been extensively studied in different cuprate systems (Crawford *et al.* 1990, Bornemann *et al.* 1992, Franck *et al.* 1993, Zhao *et al.* 1995, 1997, 1998a). For a particular family of doped cuprates the OIS increases with decreasing T_c and can be even larger than the BCS prediction. In figure 2(a), we plot the doping dependence of T_c for the ^{16}O and ^{18}O samples of the single-layer cuprate $\text{La}_{2-x}\text{Sr}_x\text{CuO}_4$ (LSCO). It is clear that the T_c values of ^{18}O samples are always lower than those of the ^{16}O samples. The doping dependence of the isotope exponent α_O is shown in figure 2(b). The magnitude of α_O increases with a decrease in doping and becomes very large (greater than 0.5) in the deeply underdoped region. The large α_O value observed near $x = 0.125$ might be related to the structural instability (Pickett *et al.* 1991). The results suggest that the phonon modes related to the oxygen vibrations are strongly coupled to conduction electrons.

In addition to the large OISs, there are also large copper-isotope shifts observed in underdoped $\text{La}_{2-x}\text{Sr}_x\text{CuO}_4$ (Franck *et al.* 1993), oxygen-depleted YBCO (Zhao *et al.* 1996c), praseodymium-substituted $\text{Y}_{1-x}\text{Pr}_x\text{Ba}_2\text{Cu}_3\text{O}_{7-y}$ (Morris *et al.* 1998) and $\text{Y}_{1-x}\text{Pr}_x\text{Ba}_2\text{Cu}_4\text{O}_8$ (Morris *et al.* 1998), as well as in $\text{YBa}_2\text{Cu}_4\text{O}_8$ (Williams *et al.* 2000). In figure 3, we plot the oxygen- and copper-isotope exponents as a function of T_c in $\text{Y}_{1-x}\text{Pr}_x\text{Ba}_2\text{Cu}_3\text{O}_{7-y}$ and $\text{Y}_{1-x}\text{Pr}_x\text{Ba}_2\text{Cu}_4\text{O}_8$. As T_c or doping decreases, both α_O and α_{Cu} increase monotonically. Interestingly, α_{Cu} is about three quarters of α_O in the deeply underdoped region, while α_{Cu} is even larger than α_O near the optimal doping. This indicates that the copper-dominated phonon modes (most of them are low-energy modes) are involved in the superconducting pairing.

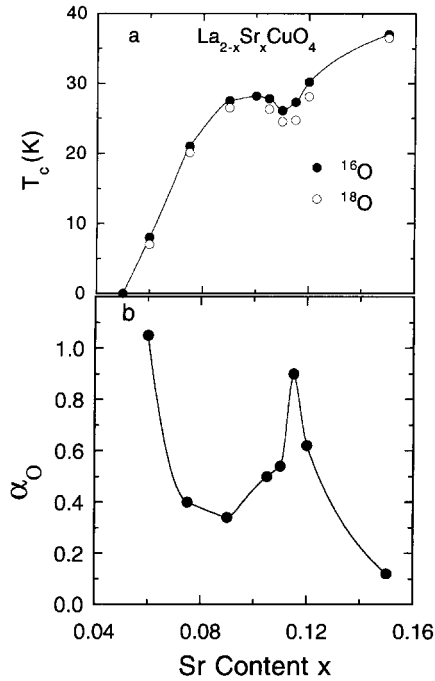


Figure 2. Dependences of T_c and the oxygen-isotope exponent α_{O} on the Sr content x for ^{16}O and ^{18}O samples of LSCO. (After Zhao *et al.* (1998a).)

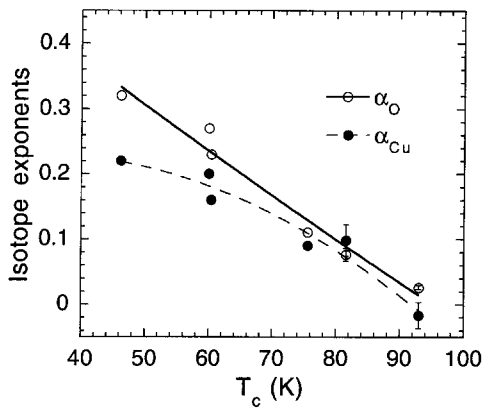


Figure 3. The oxygen and copper isotope exponents as functions of T_c for $\text{Y}_{1-x}\text{Pr}_x\text{Ba}_2\text{Cu}_3\text{O}_{7-y}$ and $\text{Y}_{1-x}\text{Pr}_x\text{Ba}_2\text{Cu}_4\text{O}_8$. The data were taken from Zhao *et al.* (1996c), Morris *et al.* (1998) and Williams *et al.* (2000).

The large copper-isotope shift also implies that the phonons in the CuO_2 planes are important to superconductivity. By analogy, one should also expect that the planar oxygen vibrations make more important contributions to the pairing than the apical and/or chain oxygen vibrations. We can distinguish between the contributions of the different oxygen sites to the total OIS in $\text{Y}_{1-x}\text{Pr}_x\text{Ba}_x\text{Cu}_3\text{O}_{7-y}$ by the site-selective oxygen-isotope experiments (Zhao *et al.* 1996a). The experimental difficulty

in the site-selective oxygen-isotope exchange was overcome by Nickel *et al.* (1993). In their experiment Nickel *et al.* replaced ^{18}O by ^{16}O in the chain and apical oxygen sites of a fully ^{18}O exchanged $\text{YBa}_2\text{Cu}_3\text{O}_7$ sample, while keeping the ^{18}O unexchanged in the plane sites. The site selectivity was confirmed by Raman spectroscopy. A small negative OIS ($\alpha_{\text{O}} = -0.01 \pm 0.004$) associated with the planar oxygen was found. In contrast, Zech *et al.* (1994) carried out a more careful experiment and showed a small positive OIS related to the planar oxygen. The above discrepancy may be due to a broad superconducting transition in the samples used by Nickel *et al.* (1993), which makes it difficult to define T_c reliably. Although the OIS is small in the optimally doped samples, the careful experiment made by Zech *et al.* (1994) has given evidence that the planar oxygen mainly contributes to the total OIS. Nevertheless it is not obvious that the same conclusion should apply to the underdoped samples where the total OIS is large. If this is the case, many theories for high- T_c superconductivity can be ruled out. Therefore studies of the site-selective oxygen isotope effect in underdoped samples will place more serious constraints on the high- T_c pairing mechanism. This was successfully done in the underdoped and optimally doped samples of $\text{Y}_{1-x}\text{Pr}_x\text{Ba}_2\text{Cu}_3\text{O}_{7-y}$ by Zhao *et al.* (1996a). In figure 4, we show the results of the site-selective oxygen-isotope effect for $\text{YBa}_2\text{Cu}_3\text{O}_{6.94}$. The data for

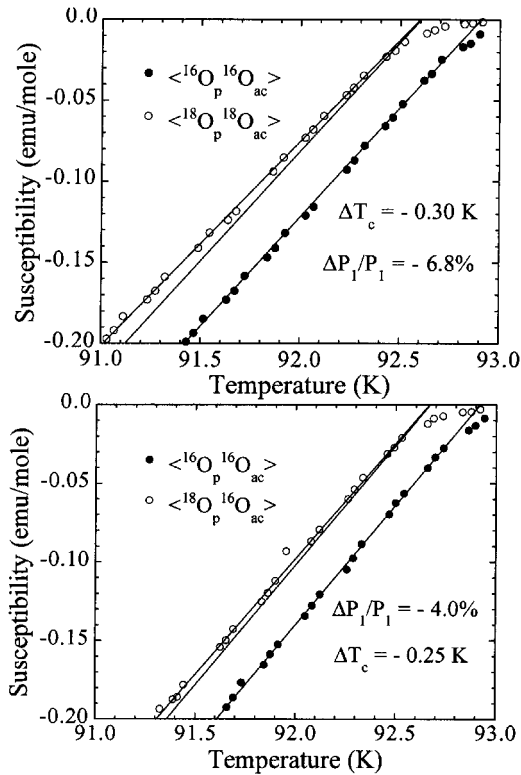


Figure 4. The site-selective oxygen-isotope effect in $\text{YBa}_2\text{Cu}_3\text{O}_{6.94}$. Here $\langle ^{18}\text{O}_p \text{ } ^{18}\text{O}_{ac} \rangle$ means all the oxygen sites are exchanged by ^{18}O , and $\langle ^{18}\text{O}_p \text{ } ^{16}\text{O}_{ac} \rangle$ means that only the in-plane oxygen sites are replaced by ^{18}O . It is evident that the planar oxygen mainly (greater than 80%) contributes to the total OIS in the optimally doped cuprate. (After Zhao *et al.* (1996a).)

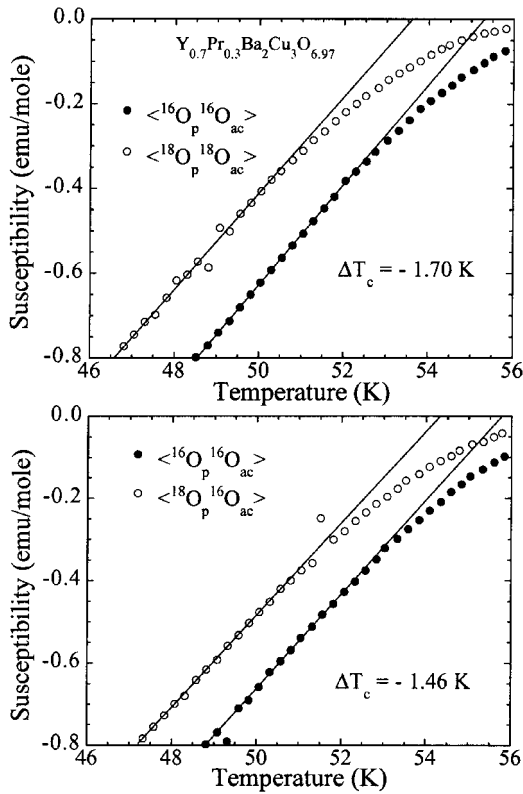


Figure 5. The site-selective oxygen-isotope effect in $Y_{0.7}Pr_{0.3}Ba_2Cu_3O_{6.97}$. The results show that the planar oxygen mainly (greater than 80%) contributes to the total OIS in this underdoped cuprate. (After Zhao *et al.* (1996a).)

$Y_{0.7}Pr_{0.3}Ba_2Cu_3O_{6.97}$ are plotted in figure 5. It is apparent that the planar oxygen mainly (greater than 80%) contributes to the total OIS in both optimally doped and underdoped samples.

2.2. Negligible oxygen-isotope effect on the carrier density

An important question may arise of whether the observed large isotope shifts in underdoped cuprates are caused by a possible difference between the carrier densities of two isotope samples or by a strong electron–phonon coupling. The former cause is very unlikely because the T_c values of ${}^{18}O$ samples are always lower than the ${}^{16}O$ samples by more than 1 K in the underdoped region, independent of whether dT_c/dx is positive, negative or zero (see figure 2 (a)).

There are two indirect experiments which have demonstrated that the difference in the hole densities of the ${}^{16}O$ and ${}^{18}O$ samples is smaller than 0.0002 per cell (Zhao *et al.* 1997, 1998a). Now we are able to determine the oxygen content very accurately using a very precise volumetric analysis (Conder *et al.* 1989). Figure 6 shows the oxygen contents of the ${}^{16}O$ and ${}^{18}O$ samples of LSCO with different doping levels x . It is remarkable that the oxygen contents of two isotope samples are the same within ± 0.0002 per cell. These indirect and direct experiments consistently show that the difference between the hole densities of the ${}^{16}O$ and ${}^{18}O$ samples is negligible, so that

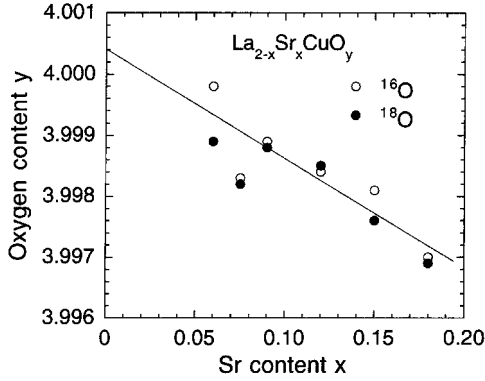


Figure 6. The oxygen contents of the ^{16}O and ^{18}O samples of LSCO with different doping levels x (unpublished data). The oxygen content was determined from a very precise volumetric analysis (Conder *et al.* 1989). The mass of each sample used for the analysis is about 500 mg. The oxygen content can be determined more precisely for a higher x and a heavier sample. The oxygen contents of two isotope samples are the same within ± 0.0002 per cell.

the observed large isotope effects are intrinsic and caused by a strong electron–phonon interaction.

2.3. Large oxygen-isotope effect on the effective supercarrier mass

Several groups have noted that there is an isotope effect on the diamagnetic Meissner signal in decoupled fine-grained samples. Zhao *et al.* (1995) seriously studied this effect and interpreted it as due to the isotope-mass dependence of the average supercarrier mass m^{**} ($\equiv [(m_{ab}^{**})^2 m_c^{**}]^{1/3}$). Since the magnetic penetration depth $\lambda(0)$ is proportional to $(m^{**}/n_s)^{1/2}$, then

$$\frac{\Delta m^{**}}{m^{**}} = \frac{2 \Delta \lambda(0)}{\lambda(0)} + \frac{\Delta n_s}{n_s}, \quad (3)$$

where Δ means any small change in a quantity upon isotope substitution. Thus the isotope dependence of m^{**} can be determined if one can independently measure the isotope dependence of $\lambda(0)$ and of n_s . As shown above, there is a negligible oxygen-isotope effect on the normal carrier density n , and $n_s = n$ for clean superconductors, so one should expect that there is no significant isotope effect on n_s .

The isotope dependence of $\lambda(0)$ can be determined from that of the Meissner fraction $f(0)$ which, for decoupled and fine-grained samples, depends on the penetration depth $\lambda(0)$ and on the average grain radius r , as seen from the Shoenberg (1940) formula for spherical grains:

$$f(T) = \frac{3}{2} \left[1 - 3 \frac{\lambda(T)}{r} \coth \left(\frac{r}{\lambda(T)} \right) + 3 \left(\frac{\lambda(T)}{r} \right)^2 \right], \quad (4)$$

where $\lambda(T) = \{[(\lambda_{ab}(T))^2 \lambda_c(T)]^{1/3}$ for layered compounds (Kogan *et al.* 1988). From equation (4), one can see that a change in $\lambda(0)$ will lead to a change in $f(0)$; so the isotope dependence of $\lambda(0)$ can be determined from the isotope dependence of $f(0)$.

In figure 7, we show the Meissner effects for the ^{16}O and ^{18}O samples of LSCO with $x = 0.06$ and 0.105 . The samples are loosely packed with rather small grain sizes ($r \approx 2\text{--}4\ \mu\text{m}$). One can clearly see that there are large oxygen-isotope effects on both T_c and the Meissner fraction. The most remarkable result is that the Meissner fraction of the ^{18}O sample is lower than for the ^{16}O sample by about 23% in the case of $x = 0.06$. The isotope effects are reversible upon the isotope back exchange (Zhao *et al.* 1997, 1998a), and reproducible in several sets of the samples. For $x = 0.06$, we evaluate $\Delta m^{**}/m^{**} = 24(2)\%$, that is there is a large negative oxygen-isotope effect on the effective supercarrier mass in the deeply underdoped cuprates. Moreover, a substantial $\Delta m^{**}/m^{**}$ value of 5–6% was also observed in several optimally doped cuprates (Zhao *et al.* 1997, Zhao and Morris 1995) although $\Delta T_c/T_c$ is small. The results clearly suggest that there exist polaronic carriers in all the doping levels, and that these carriers condense into supercarriers. It is also clear that the polaronic effects are reduced with increasing x .

The above results were obtained from powder samples and thus reflect the average properties of those highly anisotropic superconductors. To gain more insight into the role of polaronic effects, it is essential to determine the oxygen-isotope effect on the in-plane effective supercarrier mass m_{ab}^{**} . Although we have tentatively extracted the isotope dependence of m_{ab}^{**} from experiments on power samples

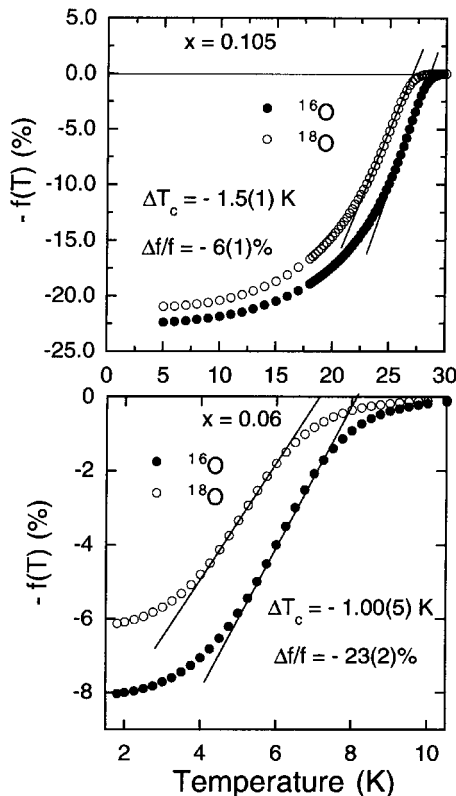


Figure 7. The Meissner fractions for the ^{16}O and ^{18}O samples of LSCO with $x = 0.06$ and 0.105 . (After Zhao *et al.* (1997, 1998a).)

(Zhao *et al.* 1997), more reliable results should be obtained from experiments on single crystals.

Unfortunately, a complete oxygen-isotope exchange by gas diffusion is impossible in single crystals with a large volume. In order to reach a complete oxygen-isotope exchange, microcrystals with a volume $V \approx 150 \mu\text{m} \times 150 \mu\text{m} \times 50 \mu\text{m}$ (mass $10 \mu\text{g}$) should be used. In this case, commercial superconducting quantum interference device magnetometers do not have enough sensitivity to measure the magnetization for such tiny crystals especially near T_c . Fortunately our highly sensitive torque magnetometer (Willemin *et al.* 1998a) is able to detect the small diamagnetic signal for the tiny crystals.

The superconducting transition was studied by cooling the sample in a magnetic field $B_a = 0.1 \text{ T}$ applied at an angle of 45° with respect to the c axis (Hofer *et al.* 2000a). The torque signal was continuously recorded upon cooling the sample at a cooling rate of 0.01 K s^{-1} . In order to determine the background signal of the cantilever, the measurement was repeated in zero field and the data were subtracted from those of the field-cooled measurement. The magnetic torque versus temperature plots obtained for the crystals with $x = 0.086$ and 0.080 are shown in figure 8. Clearly, T_c is lower for the ^{18}O -exchanged samples. Furthermore, the magnetic signals of the back-exchanged samples (crosses) coincide with those of the ^{16}O annealed samples (open circles). We define T_c as the temperature where the linearly extrapolated transition slope intersects the base line. The relative changes in T_c are found to be $\Delta T_c/T_c = -5.5(4)\%$ for $x = 0.080$ and $\Delta T_c/T_c = -5.1(3)\%$ for $x = 0.086$. The

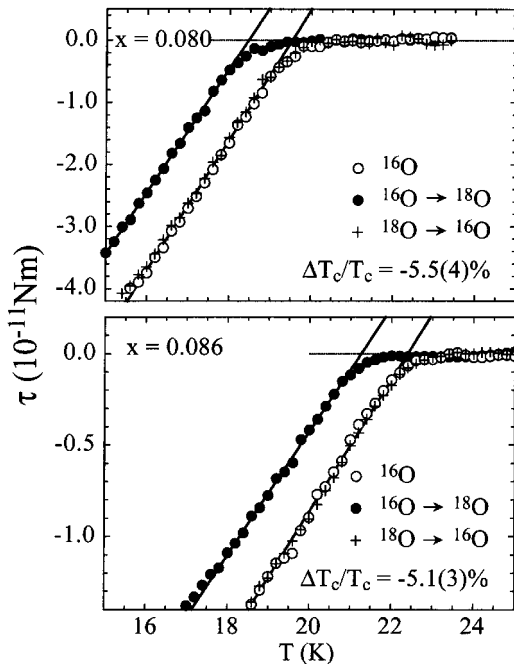


Figure 8. The magnetic torque as a function of temperature for the ^{16}O and ^{18}O microcrystals of LSCO with $x = 0.086$ and 0.080 . The measurements were carried out in a magnetic field $B_a = 0.1 \text{ T}$ applied at an angle of 45° with respect to the c axis. (After Hofer *et al.* (2000a).)

exponent α_O is found to 0.47(2) for $x = 0.080$ and 0.40(2) for $x = 0.086$, which is in good agreement with the results obtained for powder samples with similar doping levels (Crawford *et al.* 1990, Zhao *et al.* 1998a).

More interestingly, the in-plane penetration depth $\lambda_{ab}(T)$ can be extracted from field-dependent measurements (Hofer *et al.* 2000a). Figure 9 displays $\lambda_{ab}^{-2}(T)$ for the isotope-exchanged crystals with $x = 0.086$ and 0.080. The temperature dependence is described by the power law $\lambda_{ab}^{-2}(T) = \lambda_{ab}^{-2}(0)[1 - T/T_c]^n$ with an exponent $n \approx 5$. From figure 9 it is evident that both T_c and $\lambda_{ab}^{-2}(0)$ shift downwards upon replacing ^{16}O by ^{18}O . The shifts are found to be $\Delta\lambda_{ab}^{-2}(0)/\lambda_{ab}^{-2}(0) = -9(3)\%$ and $-7(1)\%$ for $x = 0.080$ and 0.086 respectively. Using $\Delta n_s = 0$, we find that $\Delta m_{ab}^{**}/m_{ab}^{**} = 7(1)\%$ for $x = 0.086$, and $\Delta m_{ab}^{**}/m_{ab}^{**} = 9(3)\%$ for $x = 0.080$. These values are very close to those obtained from experiments on power samples: $\Delta m_{ab}^{**}/m_{ab}^{**} = 9(1)\%$ for $x = 0.105$ (Zhao *et al.* 1997), and $\Delta m_{ab}^{**}/m_{ab}^{**} = 12.5\%$ for $x = 0.06$ (Zhao *et al.* 1998a).

The fact that polaronic charge carriers condense into supercarriers can naturally resolve the puzzles of the doping dependence of the isotope effect on T_c . In the underdoped regime, the superconducting transition is not of a mean-field nature, so that T_c is sensitive to n_s/m_{ab}^{**} , as shown by muon-spin rotation experiments (Uemura *et al.* 1989). Thus, an anomalously large OIS of T_c in some underdoped samples is due to a large oxygen-isotope effect on m_{ab}^{**} . On the other hand, in the optimally doped regime, the superconducting transition is mean field like; so a small isotope shift in T_c can be explained by the strong-coupling phonon-mediated mechanism together with the polaronic effects (see §6). The polaronic effects

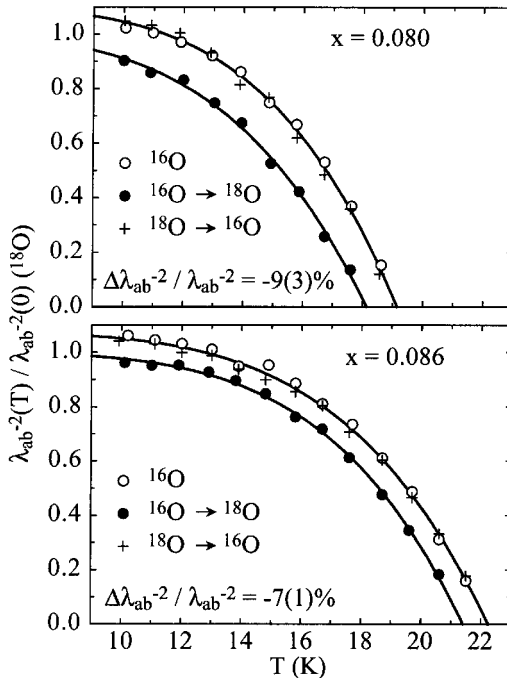


Figure 9. The in-plane penetration depth $\lambda_{ab}^{-2}(T)$ for the ^{16}O and ^{18}O microcrystals of LSCO with $x = 0.086$ and 0.080. The $\lambda_{ab}^{-2}(T)$ value was extracted from the field dependence of the torque. (After Hofer *et al.* (2000a).)

make the electron–phonon coupling constant depend on the isotope mass, leading to a negative contribution to the isotope effect on T_c , which may reduce the exponent of the isotope effect on T_c to a small value.

2.4. Huge oxygen-isotope effect on the charge stripe formation temperature

One of the most important features in the high-temperature copper oxide superconductors is the formation of alternating spin and charge stripes below a characteristic temperature (Tranquada *et al.* 1995, Mook *et al.* 1998). X-ray absorption spectroscopy measurements (Bianconi *et al.* 1996) suggested that the local structures in the alternating stripes are different, forming an incommensurate superlattice. Such a stripe phase is believed to be important to the understanding of the pairing mechanism of high-temperature superconductivity (Emery *et al.* 1997). However, the microscopic origin of the stripe phase is still highly debated. It could be caused by purely electronic interactions and/or by a strong electron–phonon interaction.

Although there is increasing experimental evidence for a strong electron–phonon interaction in the cuprate superconductors, it is not clear whether this interaction is important to the formation of the stripe phase. For the manganites with colossal magnetoresistivity, a strong electron–phonon interaction plays an essential role in the formation of the Jahn–Teller paired stripes (or charge ordering), as implied by a very large OIS in the charge-ordering temperature observed in both $\text{Nd}_{0.5}\text{Sr}_{0.5}\text{MnO}_3$ and $\text{La}_{0.5}\text{Ca}_{0.5}\text{MnO}_3$ systems (Zhao *et al.* 1998b, 1999). Therefore it is natural to ask whether the stripe formation temperature in cuprates could also depend on the oxygen-isotope mass if lattice vibrations are strongly coupled to charge carriers.

X-ray absorption near-edge spectroscopy (XANES) is a powerful technique for probing the local structure conformations for a system. There are two characteristic peaks denoted by A and B in the XANES spectra of the cuprates, which characterize the local structures within and out of the CuO_2 planes. A parameter R is defined as $R = (\beta_1 - \alpha_1)/(\beta_1 + \alpha_1)$, where β_1 and α_1 are the intensities of peak A and peak B respectively in the XANES spectra. When a charge-stripe ordering takes place, a change in the local structures leads to a sudden increase in R below the charge-stripe formation temperature T^* . The identification of T^* by XANES has been tested in an extensively studied compound $\text{La}_{1.875}\text{Ba}_{0.125}\text{CuO}_4$ (Lanzara *et al.* 1999). In figure 10, we show the temperature dependence of the parameter R for the oxygen-isotope exchanged $\text{La}_{1.94}\text{Sr}_{0.06}\text{CuO}_4$. From the figure, one can clearly see that, upon replacing ^{16}O with ^{18}O , the charge-stripe formation temperature T^* in this cuprate increases from about 110 to 180 K. Such a huge OIS of T^* indicates that a strong electron–phonon interaction is one of the driving forces for the charge-stripe formation.

The correlation between the stripe formation and superconductivity has recently been addressed by Bianconi *et al.* (2000). They determined the stripe formation temperatures for various optimally doped systems with different microstrains using polarized copper K-edge absorption measurements. The important finding is that the highest T_c is achieved in a system where the stripe instability just starts to disappear. This implies that superconductivity and stripe formation are competing with each other. The result is also consistent with the conventional picture where superconductivity is competing with charge ordering or structural instability so that the highest T_c occurs near the charge and/or structural instability.

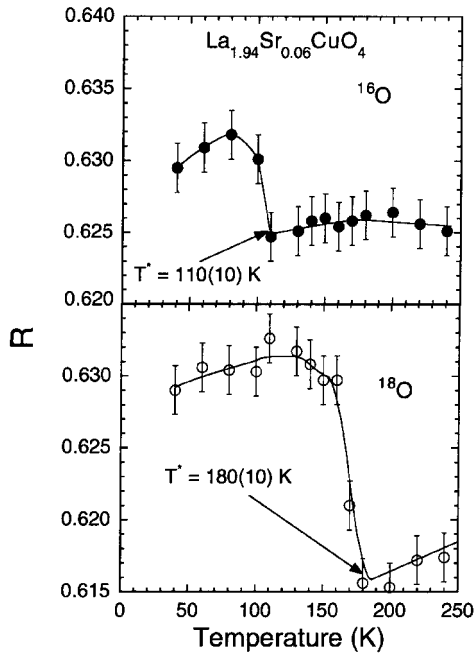


Figure 10. The temperature dependence of the parameter R for the oxygen-isotope-exchanged $\text{La}_{1.94}\text{Sr}_{0.06}\text{CuO}_4$. See text for the definition of the parameter R . (After Lanzara *et al.* (1999).)

2.5. Large oxygen-isotope effect on spin-glass freezing temperature

The parent compounds of the cuprate superconductors exhibit long-range three-dimensional AF order, which is rapidly destroyed as holes are doped into the CuO_2 planes. A short-range-ordered AF state exists at intermediate doping levels of $0.02 < x < 0.06$ (see figure 1). Early muon-spin rotation and neutron scattering experiments found that this magnetic state resembles a spin glass (Sternlieb *et al.* 1990). More detailed studies using ^{139}La nuclear quadrupole resonance (Cho *et al.* 1992) showed that the magnetic state in this doping regime is not a conventional spin glass, but a cluster spin glass. The understanding of how the short-range-ordered AF state affects superconductivity and how it is influenced by lattice vibrations will help to clarify the pairing mechanism of high- T_c superconductivity.

It is well known that conventional theories of magnetism neglect atomic vibrations; the atoms are generally considered as infinitely heavy and static in theoretical descriptions of magnetic phenomena, so there should be no isotope effect on magnetism. However, if charge carriers are polaronic, one might expect isotope effects on magnetic properties. This is indeed the case in the ferromagnetic manganites where a giant oxygen-isotope effect on the Curie temperature has been observed (Zhao *et al.* 1996b). The question is whether such an isotope effect also exists in cuprates.

If polaronic carriers exist in cuprates and the spin-glass freezing temperature T_g depends strongly on the charge mobility, one should expect a substantial isotope effect on T_g . Experimentally we find that T_g increases substantially when Mn^{2+} substitutes for Cu^{2+} by 2%. The substitution does not change the total hole density but increases the resistivity dramatically owing to the enhanced disorder and random

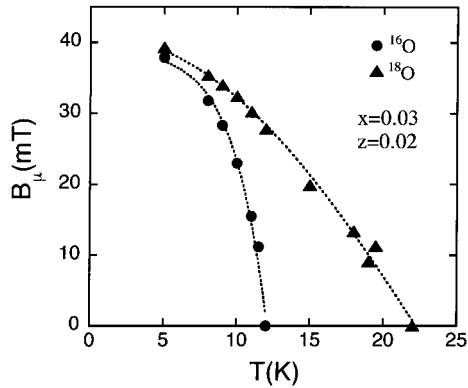


Figure 11. Temperature dependence of the internal magnetic fields B_μ (probed by muon-spin rotation) for the ^{16}O and ^{18}O samples of $\text{La}_{1.97}\text{Sr}_{0.03}\text{Cu}_{0.98}\text{Mn}_{0.02}\text{O}_4$. (After Shengelaya *et al.* (1999).)

potential in the CuO_2 planes. This may suggest that lowering the charge mobility by disorder can increase T_g . In the same way, lowering the polaron mobility by increasing the oxygen mass should lead to an increase in T_g .

In figure 11, we show the temperature dependence of the internal magnetic fields B_μ (probed by muon-spin rotation) for the ^{16}O and ^{18}O samples of $\text{La}_{1.97}\text{Sr}_{0.03}\text{Cu}_{0.98}\text{Mn}_{0.02}\text{O}_4$. It is remarkable that the spin-glass freezing temperature T_g almost doubles upon replacing ^{16}O by ^{18}O . In order to understand such an unusual isotope effect, one has to assume that the nature of charge carriers is polaronic. It is known that doped holes strongly disturb the AF bonds in the CuO_2 planes and intuitively one can expect that mobile holes are much more effective in destroying AF bonds than static holes are. In the polaronic picture, the charge carriers in the ^{18}O samples are much heavier than in ^{16}O samples. Heavier carriers are more easily trapped by a random potential; so one should expect a much lower polaron mobility in the ^{18}O samples. This can qualitatively explain the present isotope effect.

2.6. Oxygen-isotope effect on the antiferromagnetic ordering temperature

The AF ordering found in the parent insulating compounds such as La_2CuO_4 signals a strong electron–electron Coulomb correlation. On the other hand, the large isotope effects found in the underdoped cuprate superconductors indicate a strong electron–phonon interaction. The strong electron–phonon interaction in cuprates leads to the formation of polaronic carriers as shown above. Now the question arises of whether the strong electron–phonon interaction can modify the AF exchange energy and thus the AF ordering temperature in the parent insulating compounds. Studies of the isotope effect on the AF ordering temperature may help to clarify this issue.

Figures 12(a) and (b) show the temperature dependences of the susceptibility for the ^{16}O and ^{18}O samples of undoped La_2CuO_4 and of oxygen-doped $\text{La}_2\text{CuO}_{4+y}$ respectively. One can see that the AF ordering temperature T_N for the ^{18}O sample is lower than the ^{16}O sample by about 1.9 K in the case of the undoped samples. For the oxygen-doped samples, there is a negligible isotope effect. We further showed that there is no significant OIS of T_N in other undoped cuprates having no apical

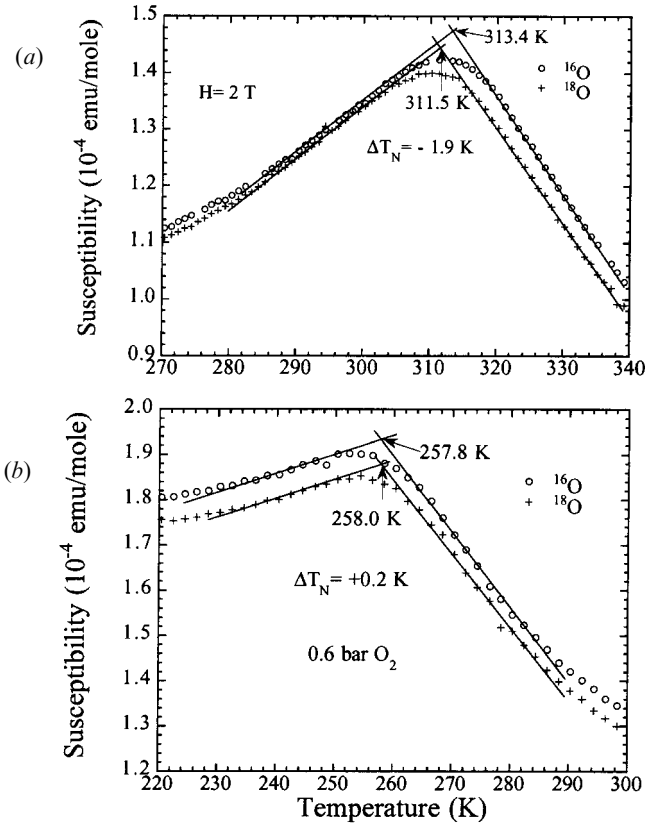


Figure 12. The temperature dependence of the susceptibility for the ^{16}O and ^{18}O samples of (a) undoped La_2CuO_4 and (b) the oxygen-doped $\text{La}_2\text{CuO}_{4+y}$. (After Zhao *et al.* (1994).)

oxygen (Zhao *et al.* 1994). This implies that lattice vibrations related to the apical oxygen is mainly responsible for the isotope effect.

It is known that the antiferromagnetism in $\text{La}_2\text{CuO}_{4+y}$ can be well described by the mean-field theory which leads to the T_N formula (Thio *et al.* 1988)

$$k_B T_N = J' \left(\frac{\xi(T_N)}{a} \right)^2, \quad (5)$$

where J' is the interlayer coupling energy and $\xi(T_N)$ is the in-plane AF correlation length at T_N given by $\xi(T_N) \propto \exp(J/T_N)$ for $y = 0$ (J is the in-plane exchange energy). When T_N is reduced to about 250 K by oxygen doping, the mesoscopic phase separation has taken place so that $\xi(T_N) = L$ (Cho *et al.* 1993), where L is the size of the antiferromagnetically correlated clusters and depends only on the extra oxygen content y . In this case, we have $T_N = J'L^2$. Since L is independent of the isotope mass, a negligible isotope shift in T_N in the oxygen-doped $\text{La}_2\text{CuO}_{4+y}$ suggests that J' is independent of the isotope mass. Then we easily find for undoped compounds

$$\frac{\Delta T_N}{T_N} = \frac{\Delta J}{J} \frac{B}{1+B}, \quad (6)$$

where $B = 2J/T_N \approx 10$. Then, from the measured isotope shift in T_N for the undoped samples, we obtain $\Delta J/J \approx -0.6\%$.

Theoretically, Kugel and Khomski (1980) considered the Jahn–Teller effect in a single-band Hubbard model. They showed that, for $U \gg E_p, \hbar\omega$,

$$J = \frac{2t^2}{U} \left(1 + \frac{2E_p\hbar\omega}{U^2} \right). \quad (7)$$

On the other hand, when $U \ll \hbar\omega$,

$$J = \frac{2t^2 \exp(-2E_p/\hbar\omega)}{U - 2E_p}. \quad (8)$$

Here U is the on-site Coulomb repulsion, t is the bare hopping integral, E_p is the Jahn–Teller stabilization energy and ω is the vibration frequency of the Jahn–Teller mode. If we take $t = 0.5$ eV, $J = 0.13$ eV, we obtain $U = 3.8$ eV. With $\hbar\omega = 0.1$ eV, $E_p = 1.2$ eV (Kamimura 1987), we obtain $\Delta J/J \approx -0.1\%$ from equation (7), which is a factor of about six smaller than the measured value. The discrepancy might arise because the parent compound is not a Hubbard insulator but a charge-transfer insulator.

§ 3. PAIRING SYMMETRY

An unambiguous determination of the symmetry of the order parameter (OP) (pair wavefunction) in cuprates is crucial to the understanding of the pairing mechanism of high-temperature superconductivity. In recent years, many experiments have been designed to test the OP symmetry in the cuprate superconductors. However, contradictory conclusions have been drawn from different experimental techniques (Hardy *et al.* 1993, Sun *et al.* 1994, Ding *et al.* 1995, Jacobs *et al.* 1995, Tsuei *et al.* 1995, Kelley *et al.* 1996, Kendziora *et al.* 1996, Lee *et al.* 1996, Sacuto *et al.* 1997, Wei *et al.* 1998, Willemin *et al.* 1998b, Bhattacharya *et al.* 1999, Kirtley *et al.* 1999, Li *et al.* 1999, Vobornik *et al.* 1999), which can be classified into being bulk sensitive and surface sensitive. For example, the techniques to measure the magnetic penetration depth and polarized Raman scattering are bulk sensitive. ARPES is essentially a surface-sensitive technique. However, the ARPES data for BSCCO should nearly reflect the bulk properties since the cleaved top surface contains an inactive Bi–O layer, and the superconducting coherent length along the c axis is very short. The single-particle tunnelling experiments can probe the bulk electronic density of states when the mean free path is far larger than the thickness of the degraded surface layer (Ponomarev *et al.* 1996). Therefore, the single-particle tunnelling experiments along the CuO₂ planes are almost bulk sensitive because of a large in-plane mean free path (greater than 100 Å). In contrast, the phase-sensitive experiments based on the Josephson tunnelling are rather surface sensitive, so that they might not probe the intrinsic bulk superconducting state if the surfaces are strongly degraded. In this case, the observed product $I_c R_N$ of the critical current multiplied by the junction normal-state resistance will be very small compared with the Ambegaokar–Baratoff limit. Then the OP symmetry at surfaces may be different from that in the bulk (Bahcall 1996). Therefore, the surface- and phase-sensitive experiments do not necessarily provide an acid test for the intrinsic bulk OP symmetry.

Here, we identify the intrinsic bulk pairing symmetry for both electron- and hole-doped cuprates from the existing bulk- and nearly bulk-sensitive experimental results such as the magnetic penetration depth, Raman scattering, single-particle tunnelling, Andreev reflection, nonlinear Meissner effect, neutron scattering and ARPES. These experiments consistently show that the dominant bulk pairing symmetry in hole-doped cuprates is of an extended s-wave type with eight line nodes, and of an s-wave type in electron-doped cuprates. The proposed pairing symmetries do not contradict with some surface- and phase-sensitive experiments which show a d-wave pairing symmetry at the degraded surfaces. We also quantitatively explain the phase-sensitive experiments along the c axis for both BSCCO and YBCO.

3.1. The order parameter symmetry in $\text{Bi}_2\text{Sr}_2\text{CaCu}_2\text{O}_{8+y}$

We first examine the high-resolution ARPES data obtained for BSCCO crystals (Ding *et al.* 1995, Vobornik *et al.* 1999). From the ARPES data, one can determine the angle dependence of the superconducting gap with a resolution as high as ± 2 meV (Vobornik *et al.* 1999). Owing to the complication arising from a possible superlattice contribution in the X quadrant, we use the data obtained for only the Y quadrant to extract the gap function. In figure 13, we show the angle dependence of the superconducting gap $\Delta(\theta)$ in the Y quadrant for slightly overdoped and heavily

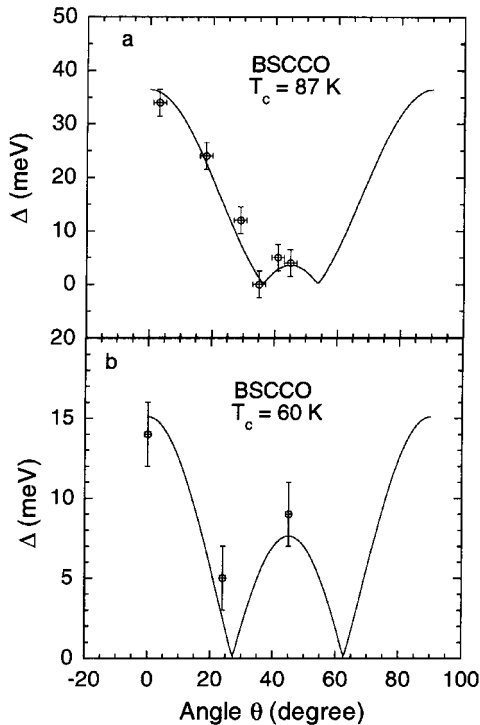


Figure 13. The angle dependence of the superconducting gap $\Delta(\theta)$ in the Y quadrant for BSCCO crystals: (a) slightly overdoped sample with $T_c = 87$ K; (b) heavily overdoped sample with $T_c = 60$ K. The magnitudes of the gap were extracted from ARPES data (Ding *et al.* 1995, Vobornik *et al.* 1999). Here θ is the angle measured from the Cu–O bonding direction.

overdoped BSCCO single crystals. The data were taken from the work of Ding *et al.* (1995) and Vobornik *et al.* (1999). Here θ is the angle measured from the Cu—O bonding direction. For the slightly overdoped sample (figure 13(a)), the gap Δ_D at $\theta = 45^\circ$ (diagonal direction) is very small (3.5 ± 2.5 meV), and the gap symmetry could be consistent with a d-wave symmetry, that is $\Delta(\theta) = \Delta \cos(2\theta)$. On the other hand, the gap along the diagonal direction (Γ –Y) for the heavily overdoped sample (figure 13(b)) is not small (9 ± 2 meV), which is obviously not consistent with the d-wave pairing symmetry. A similar evolution of the gap function with the doping has been observed by the bulk-sensitive polarized Raman scattering (Kendziora *et al.* 1996), which also shows that the difference between the magnitudes of the gaps along the Cu—O bonding direction and the diagonals becomes smaller and smaller towards overdoping.

Now the question arises as to what functional form of $\Delta(\theta)$ can fit the angle dependence of the gap shown in figure 13. In general, the gap can be expressed as $\Delta(\theta) = \Delta_s + \Delta_d \cos(2\theta) + \Delta_g \cos(4\theta) + \dots$. In the case when $\Delta_d \approx 0$, one has

$$\Delta(\theta) = \Delta[\cos(4\theta) + s], \quad (9)$$

where s is the parameter reflecting the isotropic s-wave component. This gap function has eight line nodes for $s < 1$, while there are no nodes for $s > 1$. The gap function (equation (9)) is also called the extended s-wave (denoted as the s^* -wave) function. The polarized Raman data for an optimally doped $\text{HgBa}_2\text{CaCu}_2\text{O}_{6+y}$ are in good agreement with the s^* -wave gap function (Sacuto *et al.* 1997). If we take the absolute value of $\Delta(\theta)$, then

$$|\Delta(\theta)| = |\Delta[\cos(4\theta) + s]|. \quad (10)$$

We fit the data of figure 13 by equation (10). It is remarkable that the fits are rather good. This indicates that the ARPES data may be consistent with the extended s-wave symmetry. The ARPES specified maximum gap Δ_M at $\theta = 0$ for the slightly overdoped sample is 36 ± 3 meV, which is much larger than the value (approximately 28 meV) determined from break junction spectra (Miyakawa *et al.* 1998). On the other hand, the ARPES-determined Δ_M value (15 ± 2 meV) for the heavily overdoped sample with $T_c = 60$ K is very close to the value (18 ± 2 meV) inferred from a break junction spectrum of a similar crystal with $T_c = 62$ K. The discrepancy in the former case may be due to the fact that the doping level in the top layer where the ARPES probes could be slightly lower than in the bulk (i.e. the top CuO_2 layer might be slightly underdoped). Thus, the ARPES experiments on the BSCCO single crystals are nearly bulk sensitive.

If the proposed gap functions (equations (9) and (10)) are indeed relevant, they should be also consistent with other bulk-sensitive experimental results such as the in-plane magnetic penetration depth $\lambda_{ab}(T)$. Since there are eight line nodes in the proposed gap function, the change in the in-plane penetration depth at low temperatures should be proportional to T . Following the procedure in the paper by Kosztin and Leggett (1997), we can readily show that the slope

$$\frac{d\lambda_{ab}(T)}{dT} = \frac{\lambda_{ab}(0) \ln 2}{\Delta_M} \left(\frac{1+s}{1-s} \right)^{1/2}. \quad (11)$$

Compared with the d-wave symmetry, the magnitude of the slope $d\lambda_{ab}(T)/dT$ is enhanced by a factor $[(1+s)/(1-s)]^{1/2}$. In terms of Δ_M and Δ_D , we find that

$s = (\Delta_M - \Delta_D)/(\Delta_M + \Delta_D)$ and $\Delta = (\Delta_M + \Delta_D)/2$. Then, equation (11) can be rewritten as

$$\frac{d\lambda_{ab}(T)}{dT} = \frac{\lambda_{ab}(0) \ln 2}{(\Delta_M \Delta_D)^{1/2}}. \quad (12)$$

It is interesting to see that $d\lambda_{ab}(T)/[\lambda(0) dT]$ is inversely proportional to $(\Delta_M \Delta_D)^{1/2}$, namely the geometric average of Δ_M and Δ_D . From equation (12), we can calculate $d\lambda_{ab}(T)/dT$ using the measured $\lambda_{ab}(0) = 2690 \pm 150 \text{ \AA}$ for BSCCO with $T_c = 90 \text{ K}$ (Prozorov *et al.* 2000a), and the values of Δ_M and Δ_D deduced from figure 1 (a). The calculated $d\lambda_{ab}(T)/dT$ is $14 \pm 2 \text{ \AA K}^{-1}$, which is very close to the measured value ($12 \pm 2 \text{ \AA K}^{-1}$) (Jacobs *et al.* 1995, Lee *et al.* 1996, Prozorov *et al.* 2000a). In contrast, if the pairing symmetry is d-wave, the calculated $d\lambda_{ab}(T)/dT$ is $4.5 \pm 0.6 \text{ \AA K}^{-1}$ which is a factor of three smaller than the measured value. Therefore, the extended s-wave symmetry extracted from the ARPES data is in quantitative agreement with the $\lambda_{ab}(T)$ data (Jacobs *et al.* 1995, Lee *et al.* 1996, Prozorov *et al.* 2000a).

Single-particle tunnelling spectroscopy can probe the superconducting density of states with fine energy resolution and considerable directionality. For an isotropic s-wave superconductor, the characteristic dI/dV versus V curve in the point-contact superconductor–insulator–normal-metal tunnelling junctions exhibits a step-like peak at a voltage $V_p = \Delta/e$. For an anisotropic gap function $\Delta(\theta)$, the directional dependence of the tunnelling differential conduction is given by (Suzuki *et al.* 1999a)

$$\frac{dI}{dV} \propto \int_0^{2\pi} p(\theta - \theta_0) \Re \left(\frac{eV - i\Gamma}{[(eV - i\Gamma)^2 - \Delta^2(\theta)]^{1/2}} \right) N(\theta) d\theta, \quad (13)$$

where $N(\theta)$ represents the anisotropy of the band dispersion, Γ is the lifetime broadening parameter of an electron, $p(\theta - \theta_0)$ is the angle dependence of the tunnelling probability and θ_0 is the angle of the direction perpendicular to the tunnelling barrier. According to the Wentzel–Kramers–Brillouin approximation, $p(\theta - \theta_0)$ decays exponentially as $p(\theta - \theta_0) = \exp[-\beta \sin^2(\theta - \theta_0)]$. The parameter β decreases with decreasing barrier resistance R_N . For simplicity, we assume a cylindrical Fermi surface, so that both $N(\theta)$ and β are independent of the angle. This will not change the basic features of the dI/dV curve. In figure 14 we show the numerically calculated results of the renormalized dI/dV for a gap function $\Delta(\theta) = \Delta[\cos(4\theta) + s]$ with $\Delta = 24 \text{ meV}$ and $s = 0.25$. One can readily show that the maximum gap is $\Delta_M = (1 + s)\Delta = 30 \text{ meV}$ at $\theta = 0$, and the gap along the diagonal directions is $\Delta_D = (1 - s)\Delta = 18 \text{ meV}$. From figure 14, one can see that either two or four peak features appear clearly in the dI/dV curves, depending on the tunnelling barrier direction and/or the β value. For a small β value (corresponding to a small barrier resistance), four peak features are well defined (see curve A). The peak positions are located at $eV = \pm\Delta_M$ and $\pm\Delta_D$. Therefore, from the peak positions, we can determine Δ_M and Δ_D .

In figure 15, we plot the normalized dI/dV curve at 14 K for a superconductor–insulator–superconductor (SIS) break junction on a BSCCO crystal which is slightly overdoped ($T_c = 90 \text{ K}$) (Mourachkine 1999). The junction has a very low barrier resistance (about 200 \Omega) (Mourachkine 1999), indicating a small β value. It is remarkable that there are four well-defined peak features in the spectrum, which resembles curve A in figure 14. When the barrier resistance is above $2 \text{ k}\Omega$, the inner

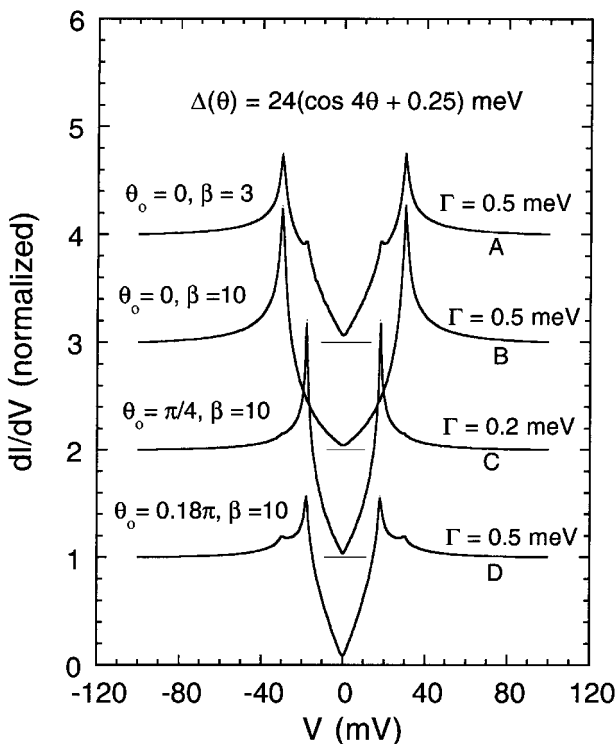


Figure 14. Numerically calculated curves of the renormalized dI/dV for a gap function of $\Delta(\theta) = \Delta[\cos(4\theta) + s]$ with $\Delta = 24$ meV and $s = 0.25$. The four curves correspond to different values of the parameters Γ , β and θ_0 , which are indicated in the figure. Curves A, B and C are vertically shifted up by 3, 2 and 1 respectively.

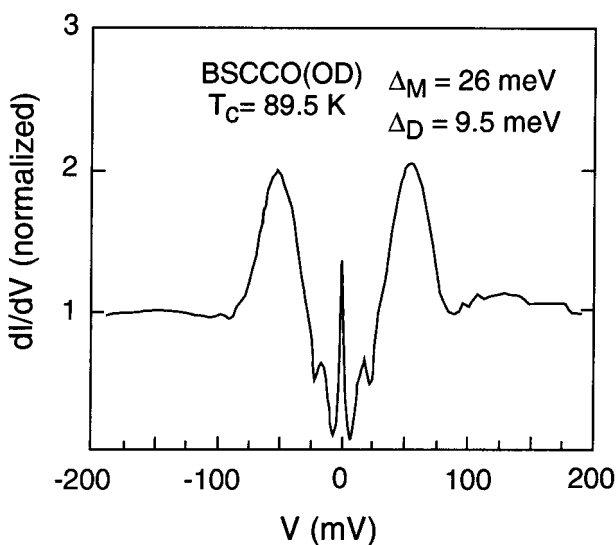


Figure 15. Normalized dI/dV curves at 14 K for the SIS break junctions on a slightly overdoped BSCCO crystal. The spectra were taken from the paper by Mourachkine (1999).

gap features disappear (Mourachkine 1999), in agreement with curve B in figure 14. We would like to mention that, for SIS break junctions, the peak positions are located at $eV = \pm 2\Delta_M$ and $\pm 2\Delta_D$. From the spectra, we obtain $\Delta_M = 26 \pm 0.5$ meV and $\Delta_D = 9.5 \pm 0.5$ meV. The Δ_M value obtained from the break junction spectrum is the same as that found from the c -axis intrinsic tunnelling junction made of the insulating Bi–O layers (Müller *et al.* 2000). From the Δ_M and Δ_D values, we deduce a gap function $\Delta(\theta) = \Delta[\cos(4\theta) + s]$ with $\Delta = 17.75$ meV and $s = 0.46$. Similarly, the earlier break junction spectra for overdoped BSCCO with $T_c = 86$ K also indicate double-gap features at $\Delta_M = 24 \pm 2$ meV and at $\Delta_D = 12 \pm 1$ meV (Buschmann *et al.* 1992). The tunnelling spectra are in good agreement with ARPES data for overdoped BSCCO with $T_c = 83$ K (Ma *et al.* 1995). The ARPES experiment clearly showed that $\Delta_M = 20 \pm 2$ meV and $\Delta_D = 12 \pm 2$ meV (Ma *et al.* 1995). Moreover, the inner gap features also appear in the SIS break junction spectra of a heavily overdoped crystal with $T_c = 62$ K, corresponding to $\Delta_D = 7.5$ – 9.0 meV (DeWilde *et al.* 1998, Ozyuzer *et al.* 2000). The magnitude of Δ_D is in excellent agreement with that found from ARPES experiment (see figure 13 (b)).

We would like to point out that the values of Δ_M determined from Raman spectrum of B_{1g} symmetry may be overestimated because the extended van Hove singularity is slightly below the Fermi level. In this case, the spectra would show double peaks at Raman shifts of $2\Delta_M$ and $2(\Delta_M^2 + \xi_{vH}^2)^{1/2}$, where ξ_{vH} is the energy position of the van Hove singularity below the Fermi level. When $\xi_{vH} \ll \Delta_M$, one can only see a single broad peak close to $2(\Delta_M^2 + \xi_{vH}^2)^{1/2}$ owing to a high density of states at the extended van Hove singularity.

3.2. The order parameter symmetry in $YBa_2Cu_3O_{7-y}$

Evidence for an extended s -wave pairing symmetry in YBCO also comes from the single-particle tunnelling spectra. Figure 16 shows the scanning tunnelling spectrum for a slightly overdoped YBCO crystal (Maggio-Aprile *et al.* 1995). Four peak features appear in this spectrum, which is similar to curve D in figure 14. From the peak positions, we obtain $\Delta_M = 30 \pm 2$ meV and $\Delta_D = 19 \pm 1$ meV. The size of $\Delta_M \approx 30$ meV is consistent with a break junction spectrum (Ponomarev *et al.* 1996),

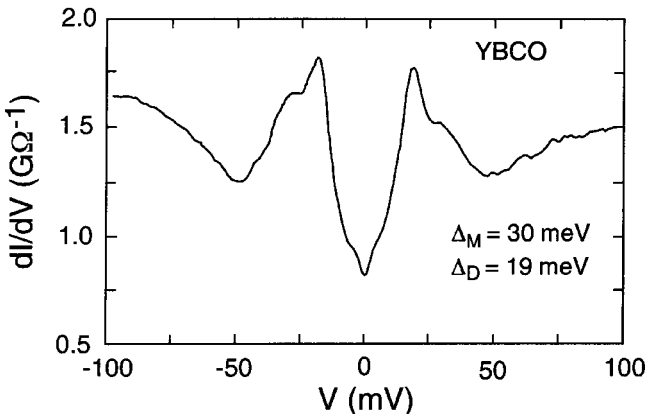


Figure 16. Scanning tunnelling spectrum for a slightly overdoped YBCO crystal. The spectrum was taken from the paper by Maggio-Aprile *et al.* (1995).

and a scanning tunnelling spectrum along the a -axis direction (Wei *et al.* 1998). A gap feature with $\Delta_D = 19$ meV was also seen in a scanning tunnelling spectrum (Wei *et al.* 1998) which is very similar to curve C in figure 14.

Now we discuss the Andreev reflection. Since there is sign change about its nodal directions in our extended s-wave OP, the Andreev-bound surface states can be formed. This will lead to a zero-bias conduction peak if tunnelling is nearly along one of the nodal directions and the Fermi velocities between the cuprates and normal metals (e.g. silver and gold) are well matched. For hole-doped cuprates, the Fermi velocity v_F strongly depends on the angle θ , that is v_F is low along the bonding direction, and high along the diagonal directions. This implies that the observation of the Andreev reflection is difficult for tunnelling along the bonding direction since the value of v_F along this direction is low compared with that of gold or silver. Owing to the strong anisotropy of v_F in cuprates, the Andreev reflection mainly probes the gap feature at $eV = \Delta_D$. If tunnelling is along one of the diagonal directions, and the angle between the nodal and diagonal directions is far larger than the tunnelling half-angle (depending on β), one can see an s-wave-like gap approximately equal to Δ_D in the Andreev reflection spectra. Indeed an s-wave-like gap feature at $eV \approx 20$ meV has been observed in the Andreev reflection spectra of several YBCO crystals with $T_c = 90$ K (Yagil *et al.* 1995). We would like to mention that, in general, the double-gap features should also appear in the Andreev reflection spectra when the β value is small.

The tunnelling data of YBCO (figure 16) are thus consistent with a gap function $\Delta(\theta) = \Delta[\cos(4\theta) + s]$ with $\Delta = 24.5$ meV and $s = 0.225$. This gap function is in quantitative agreement with the a -axis penetration depth data (which reflect magnetic screening in CuO_2 planes) for a fully oxygenated YBCO crystal (Kamal *et al.* 1998). From equation (12), we calculate $d\lambda_a(T)/dT = 4.0 \text{ \AA K}^{-1}$ by using $\lambda_a(0) = 1600 \text{ \AA}$ (Kamal *et al.* 1998), $\Delta_D = 19$ meV, and $\Delta_M = 30$ meV. We shall obtain the same value of $d\lambda_a(T)/dT$ if we use $\Delta_D = 21$ meV and $\Delta_M = 27$ meV. The measured value of $d\lambda_a(T)/dT$ is 4 \AA K^{-1} (Kamal *et al.* 1998).

Now we calculate the temperature dependence of $\lambda_{ab}^2(0)/\lambda_{ab}^2(T)$ for the s*-wave gap function. For a cylindrical Fermi surface (Jacobs *et al.* 1995)

$$\frac{\lambda_{ab}^2(0)}{\lambda_{ab}^2(T)} = 1 + \frac{1}{\pi} \int_0^{2\pi} \int_0^\infty d\theta d\epsilon \frac{\partial f}{\partial E}. \quad (14)$$

Here $E = [\epsilon^2 + \Delta^2(\theta, T)]^{1/2}$, f is the Fermi–Dirac distribution function, $\Delta(\theta, T) = \Delta(T)[\cos(4\theta) + s]$ and $\Delta(T) = \Delta \tanh[2.2(T/T_c - 1)^{1/2}]$ (Thelen *et al.* 1993). In figure 17, we compare the experimental data for YBCO (open circles) (Kamal *et al.* 1998) and the numerically calculated result (solid curve) for the above-deduced gap function $\Delta(\theta) = 24.5[\cos(4\theta) + 0.225]$ meV. It is remarkable that the data are in quantitative agreement with the calculated result without any fitting parameters. The broken curve is the calculated result for a d-wave gap function $\Delta(\theta) = \Delta_M \cos(2\theta)$ with $\Delta_M = 30$ meV. It is clear that the agreement between the data and the calculated curve is poor for the d-wave symmetry.

The gap function of YBCO deduced from the tunnelling and the $\lambda_a(T)$ data is also consistent with the measured transverse magnetization m_T in the Meissner state (Bhattacharya *et al.* 1999), as plotted in figure 18. This bulk-sensitive experiment shows a very small sine fourfold component of the transverse magnetization, which is at least four times smaller than the predicted value from the d-wave symmetry.

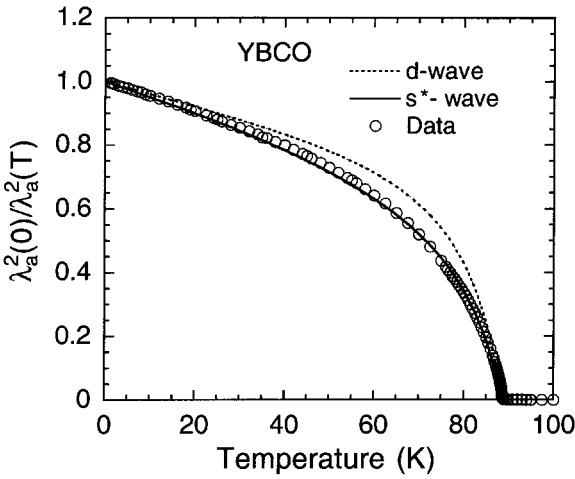


Figure 17. Temperature dependence of the a -axis $\lambda_a^2(0)/\lambda_a^2(T)$ for a very high-quality YBCO crystal with $T_c = 88.7\text{K}$: (—), calculated curve for the s^* -wave gap function deduced from the tunnelling spectrum in figure 16; (- - -), calculated curve for a d -wave gap function with $\Delta_M = 30\text{meV}$. The data were taken from the paper by Kamal *et al.* (1998).

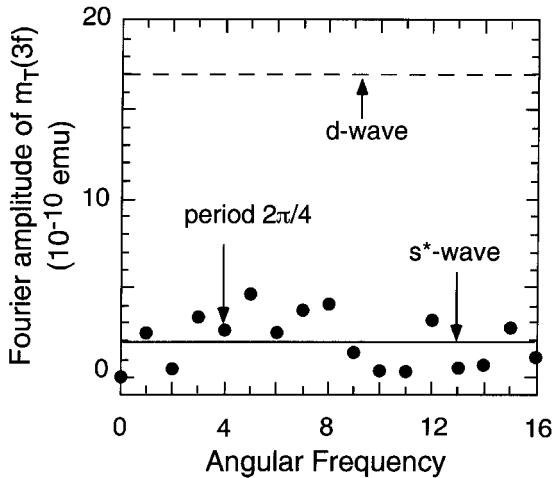


Figure 18. Sine Fourier amplitudes of the transverse magnetization m_T in the Meissner state for a high-quality YBCO crystal: (—) predicted sine Fourier amplitude at $2\pi/4$ for the s^* -wave gap function deduced from the tunnelling spectrum in figure 16 and the a -axis $\lambda_a(T)$ data in figure 17; (- - -), predicted amplitude for a d -wave gap function. The data were taken from the paper by Bhattacharya *et al.* (1999).

This indicates that the dominant pairing symmetry is not of a d -wave type. Using the formulae in the paper by Zutic and Valls (1997), we can calculate the fourfold sine component of the transverse magnetization for the s^* -wave gap function deduced above. We find that the value of m_T for the s^* -wave OP is a factor of 8.9 smaller than for the pure d -wave OP. The predicted sine Fourier amplitude at period $2\pi/4$ is indicated by a horizontal solid line in figure 18. It is clear that the predicted amplitude is below the noise level, which is about $5 \times 10^{-10}\text{emu}$ (Bhattacharya *et al.*

1999). Therefore, the negligibly small nonlinear Meissner effect observed in YBCO is in agreement with the s*-wave OP rather than with the d-wave OP.

3.3. The order parameter symmetry in $\text{La}_{2-x}\text{Sr}_x\text{CuO}_4$

The polarized Raman scattering data (Chen *et al.* 1994) for nearly optimally doped LSCO with $T_c = 37\text{ K}$ yield $2\Delta_M/k_B T_c = 7.7$. From the measured value of $d\lambda_{ab}(T)/[\lambda_{ab}(0)dT]$ for the optimally doped LSCO (Panagopoulos *et al.* 1999), one can readily calculate $2(\Delta_M \Delta_D)^{1/2}/k_B T_c = 4.2$ using equation (12). Then we find $2\Delta_D/k_B T_c = 2.3$, that is $\Delta_D = 3.8\text{ meV}$. This value is in good agreement with the Andreev reflection spectrum of an optimally doped LSCO (Deutscher *et al.* 1997), which shows an s-wave-like gap feature at $eV \approx 3.5\text{ meV}$. Therefore, three independent bulk-sensitive experiments on optimally doped LSCO consistently suggest a gap function $\Delta(\theta) = 8.1[\cos(4\theta) + 0.53]\text{ meV}$ with $\Delta_D = 3.8\text{ meV}$ and $\Delta_M = 12.5\text{ meV}$.

Now we can quantitatively explain the neutron scattering experiment on an optimally doped LSCO single crystal (Lake *et al.* 1999). The experiment shows that low-energy magnetic excitations are peaked at the quartet of wave-vectors $(0.5 \pm 0.135, 0.5)$ and $(0.5, 0.5 \pm 0.135)$ in the normal state, and a spin gap with an energy of about 6.7 meV appears in the low-temperature superconducting state. The magnitude of the spin gap should be equal to twice the superconducting gap along the incommensurate wave vectors (that is at $\theta = 39^\circ$) (Mason *et al.* 1996). From the gap function deduced above, we calculate $2\Delta(39^\circ) = 6.2\text{ meV}$, in remarkably good agreement with experiment. Moreover, it was also found (Lake *et al.* 1999) that the spin gap at $\theta = 45^\circ$ is $6 \pm 2\text{ meV}$, which is consistent with $2\Delta_D = 7.6\text{ meV}$ within the experimental uncertainty. Obviously, the d-wave gap function is incompatible with the large spin gap observed along the diagonal direction. In contrast, the s*-wave OP for LSCO is in quantitative agreement with the neutron experiment.

3.4. The order parameter symmetry in electron-doped cuprates

The recent measurements of $\lambda_{ab}(T)$ in an electron-doped $\text{Pr}_{1.85}\text{Ce}_{0.15}\text{CuO}_{4-y}$ (PCCO) reveal contradictory results (Alff *et al.* 1999, Prozorov *et al.* 2000b). In a high-quality PCCO thin film with the lowest residual resistivity and the highest T_c , the temperature dependence of $[\lambda_{ab}(T) - \lambda_{ab}(0)]/\lambda_{ab}(0)$ is consistent with an s-wave pairing symmetry with a reduced energy gap $2\Delta(0)/k_B T_c = 2.9$ (Alff *et al.* 1999). On the other hand, the low-temperature $\lambda_{ab}(T)$ in less ideal PCCO single crystals exhibits a power-law temperature dependence, as expected from a dirty d-wave superconductor (Prozorov *et al.* 2000b).

We show that these apparently conflicting data might well be reconciled by a deeper understanding of how microstructure affects screening. It is well known, for example, that the screening length in a weakly coupled Josephson array of grains is dominated by the magnitude and temperature dependence of the Josephson coupling current between array elements (Giovannini and Weiss 1978). Thus, tunnel coupling across grain boundaries and/or planar defects (weak links), rather than the BCS response of the grains themselves, mainly determines the magnetic screening length, surface resistance and critical current (see the review article by Halbritter (1999)). The extrinsic effect due to the weak links can lead to a linear T dependence in the effective $\lambda_{ab}(T)$ at low temperatures and to a large residual surface resistance (Halbritter 1992). Similarly, Hebard *et al.* (1991) showed that the current-induced nucleation of vortex-antivortex pairs at defects can make an additional extrinsic

contribution to the screening length, that is a pinning penetration depth $\lambda_{ab}^p(T)$. Within this scenario, $\lambda_{ab}(T)$ in zero magnetic field is given by (Hebard *et al.* 1991)

$$\lambda_{ab}^p(t) = \frac{\lambda_{ab}^p(0)}{1 - t^2}, \quad (15)$$

where $t = T/T_c$, $\lambda_{ab}^p(0) = [\Phi_0/H_c(0)](2N_d/\pi)^{1/2}$, Φ_0 is the flux quantum, N_d is the areal density of uniformly distributed defects and $H_c(0)$ is the zero-temperature critical field. In the presence of the external dc field H , the expression for $\lambda_{ab}^p(0, H)$ has to be modified (Halbritter 1992). The total screening length is $\lambda_{ab}(t) = \{[\lambda_{ab}^L(t)]^2 + [\lambda_{ab}^p(t)]^2\}^{1/2}$, where $\lambda_{ab}^L(t)$ is the intrinsic London penetration depth (Hebard *et al.* 1991). Assuming an s-wave pairing symmetry, we readily show that $\lambda_{ab}(T)$ at low temperatures (below $0.2\Delta(0)/k_B$) is given by

$$\lambda_{ab}(T) = \lambda_{ab}(0) + \frac{[\lambda_{ab}^L(0)]^2}{\lambda_{ab}(0)} \left(\frac{\pi\Delta(0)}{2k_B T} \right)^{1/2} \exp\left(-\frac{\Delta(0)}{k_B T}\right) + \frac{\lambda_{ab}^2(0) - [\lambda_{ab}^L(0)]^2}{\lambda_{ab}(0)T_c^2} T^2. \quad (16)$$

It is clear that the T^2 dependence of $\lambda_{ab}(T)$ at low temperatures in zero field can be completely caused by the extrinsic effect, that is the nucleation of vortex–antivortex pairs at defects. If N_d is negligible, $\lambda_{ab}(0) = \lambda_{ab}^L(0)$, and the second term in equation (16) is absent. Then we recover the BCS expression (Mühschlegel 1959)

$$\lambda_{ab}(T) = \lambda_{ab}(0) + \lambda_{ab}(0) \left(\frac{\pi\Delta(0)}{2k_B T} \right)^{1/2} \exp\left(-\frac{\Delta(0)}{k_B T}\right). \quad (17)$$

In figure 19(a), we plot the temperature dependence of $\lambda_{ab}(T)$ below 6 K for a PCCO single crystal. The data are from the paper by Prozorov *et al.* (2000b). The zero-temperature in-plane penetration depth $\lambda_{ab}(0)$ was measured to be about 2500 Å (Prozorov *et al.* 2000b). This crystal shows T_c^{onset} at 22 K (defined by the onset of diamagnetism), and T_c^{mid} at 19 K (defined as the inflection point on $\lambda_{ab}(T)$) (Prozorov *et al.* 2000b). A wide superconducting transition in this crystal manifests the rather low quality of the crystal.

We fit the data by equation (16) with two fitting parameters $\Delta(0)$ and $\lambda_{ab}^L(0)$, and with a fixed $T_c = 20.5$ K (the average of T_c^{onset} and T_c^{mid}). The solid curve is the curve fitted by equation (16). It is remarkable that the fit is very good. This can be seen more clearly in figure 19(b) where the difference between the data and the fitted curve is plotted. There is a negligible systematic error (the deviation is less than the magnitude of the data scattering). From the fit, we find that $\Delta(0)/k_B = 29.6 \pm 0.1$ K and $\lambda_{ab}^L(0) = 1643$ Å. The deduced $\lambda_{ab}^L(0)$ is in excellent agreement with the value (1600 ± 100 Å) obtained from the optical data (Homes *et al.* 1997). The magnitude of $2\Delta(0)/k_B T_c = 2.9$ is also the same as deduced from a high-quality film where the T^2 term is absent (Alff *et al.* 1999). The value of $\Delta(0)$ justifies the fit to the data below 6 K, namely $0.2\Delta(0)/k_B$. Therefore, the $\lambda_{ab}(T)$ data for the crystal are in quantitative agreement with a dominant s-wave pairing symmetry.

From the values of $\lambda_{ab}^L(0)$ and $\lambda_{ab}(0)$, we calculate $\lambda_{ab}^p(0) = 1884$ Å. Using the relation $\lambda_{ab}^p(0) = [\Phi_0/H_c(0)](2N_d/\pi)^{1/2}$ and $H_c(0) = 2$ kOe (Wu *et al.* 1993), we estimate that $N_d = 5.2 \times 10^{10}$ cm⁻², corresponding to one defect over 1333 copper sites. This implies that a small density of defects can produce quite a large $\lambda_{ab}^p(0)$, which contributes a substantial T^2 term in $\lambda_{ab}(T)$.

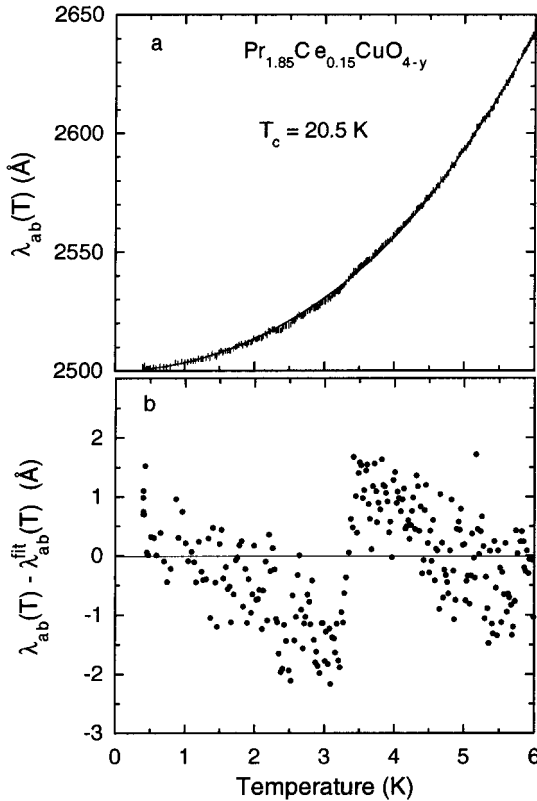


Figure 19. (a) Temperature dependence of $\lambda_{ab}(T)$ below 6 K for a PCCO single crystal: (—), fitted curve by equation (16) with $2\Delta(0)/k_B T_c = 2.9$ and $\lambda_{ab}^L(0) = 1643 \text{ \AA}$. The value of $\lambda_{ab}^L(0)$ was found to be $1600 \pm 100 \text{ \AA}$ from the optical data (Homes *et al.* 1997). (b) The difference between the data and the fitted curve. The data are from the paper by Prozorov *et al.* (2000b).

In order to rule out the possibility that the data can be also consistent with a d-wave symmetry in the dirty limit, we plot the data as $1 - \lambda_{ab}^2(0)/\lambda_{ab}^2(T)$ versus T^2 in figure 20. It is apparent that the quantity $1 - \lambda_{ab}^2(0)/\lambda_{ab}^2(T)$ is proportional to T^2 below about 5 K. For a dirty d-wave superconductor, a crossover from T^2 to T dependence should be seen at a temperature $T^* \approx [\lambda_{ab}(0) \ln 2]/[\Delta_M(0) d\lambda_{ab}/dT^2]$, where $\Delta_M(0)$ is the maximum gap at zero temperature (Hirschfeld and Goldenfeld 1993). Using $\lambda_{ab}(0) = 2500 \text{ \AA}$ (Prozorov *et al.* 2000b), $d\lambda_{ab}/dT^2 = 3.7 \text{ \AA K}^{-2}$ (Prozorov *et al.* 2000b), and $\Delta_M(0) = 2.5 T_c$ (Stadlober *et al.* 1995), one finds that $T^* \approx 9 \text{ K}$. There is no such crossover at any temperatures up to 11 K (see figure 20). Only a possible crossover from the T^2 to a higher power-law dependence is seen at about 5 K. Therefore, the data cannot agree with the d-wave pairing symmetry. Furthermore, the absence of the linear T term in $\lambda_{ab}(T)$ indicates that the extrinsic contribution to $\lambda_{ab}(T)$ due to weak links (Halbritter 1992) is negligible in this crystal.

In figure 21, we show $[\lambda_{ab}(T) - \lambda_{ab}(0)]/\lambda_{ab}(0)$ as a function of temperature for a high-quality PCCO thin film. The data are from the paper by Alff *et al.* (1999). The film has the lowest residual resistivity (less than $50 \mu\Omega \text{ cm}$) and the highest T_c (24 K) reported for the PCCO system (Alff *et al.* 1999). This indicates the high quality of the

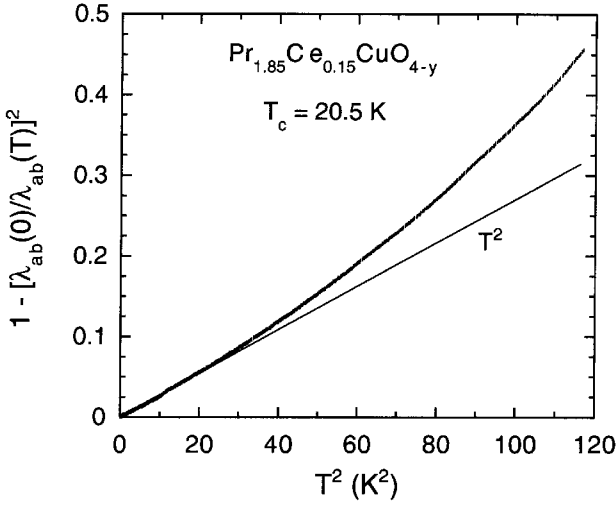


Figure 20. The T^2 dependence of the quantity $1 - \lambda_{ab}^2(0)/\lambda_{ab}^2(T)$ over 0.4–10.8 K for the same PCCO crystal as that used for figure 19. The crossover from the T^2 to a higher power-law dependence starts at about 5 K. There is no crossover from the T^2 to the T dependence at $T^* \approx 9$ K.

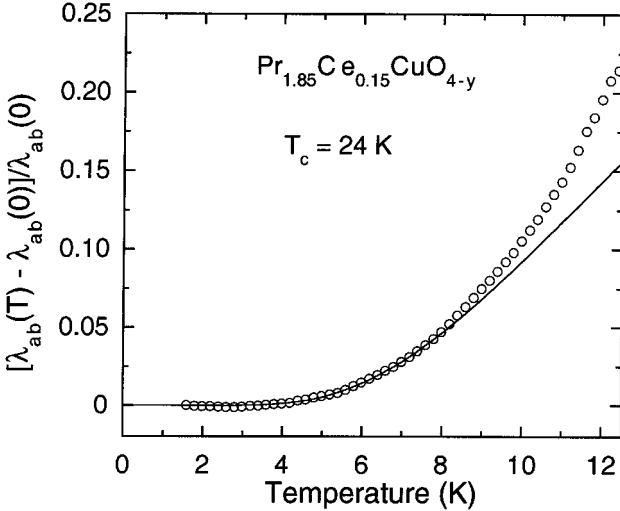


Figure 21. Temperature dependence of $[\lambda_{ab}(T) - \lambda_{ab}(0)]/\lambda_{ab}(0)$ for a high-quality PCCO thin film with the lowest residual resistivity and the highest T_c : (—), fitted curve by equation (17) with $2\Delta(0)/k_B T_c = 2.7$. The data are from the paper of Alff *et al.* (1999).

film, which was grown using molecular-beam epitaxy. The optimal quality of the film may be because homogeneous oxygen reduction can be easily achieved in thin films. Since the data at low temperatures are quite flat, it appears that there is neither a T^2 nor a T contribution. We thus fit the data below 6.5 K by equation (17) with one fitting parameter $\Delta(0)$. The best fit gives $\Delta(0)/k_B = 31.9 \pm 0.1$ K, which justifies the fit to the data below 6.5 K ($\sim 0.20\Delta(0)/k_B$). This leads to $2\Delta(0)/k_B T_c = 2.7$, which is

nearly the same as that deduced above for the less ideal crystal where there is a significant T^2 term in $\lambda_{ab}(T)$ due to the existence of defects. All these results consistently suggest that the pairing symmetry in electron-doped cuprates is anisotropic s-wave type with no line nodes.

Polarized Raman scattering (Stadlober *et al.* 1995) has also shown that the symmetry of the order parameter in $\text{Ne}_{1.84}\text{Ce}_{0.16}\text{CuO}_{4-y}$ (NCCO) is consistent with an anisotropic s wave. If we use $\Delta_M = 2.5T_c$ (Stadlober *et al.* 1995) and the minimum gap $\Delta_m = 1.4T_c$ (from the $\lambda_{ab}(T)$ data), we find that $\Delta(\theta) = 1.15[3.52 + \cos(4\theta)]\text{meV}$ for an electron-doped cuprate with $T_c = 24\text{K}$. Therefore, three bulk-sensitive experiments consistently indicate an anisotropic s-wave pairing symmetry in electron-doped cuprates.

3.5. Phase-sensitive experiments along the c -axis direction

The most reliable phase-sensitive experiment is the atomically clean BSCCO Josephson junctions between identical single-crystal cleaves stacked and twisted an angle ϕ_0 about the c axis (Li *et al.* 1999). The quality of the junction is nearly the same as that of the intrinsic Josephson junctions made of the Bi–O insulating layers. Theoretically, it has been shown that the critical current I_c of the twist junction is (Klemm *et al.* 1998)

$$I_c \propto \sum_{\ell} \eta_{\ell} \Delta_{\ell} \cos(\ell\phi_0), \quad (18)$$

where $\ell = 0, 1, 2, \dots$, and $\eta_{\ell} \ll \eta_0$ for $\ell \geq 1$. The above equation indicates that the s-wave component contributes to the critical current much more effectively. The experiment (Li *et al.* 1999) shows that the I_c value is nearly independent of the twist angle ϕ_0 , and the temperature dependence of I_c is consistent with the Ambegaokar–Baratoff model for an s-wave superconductor. This indicates that the s-wave component in this material must be significant compared with the other high-angular-momentum components. For slightly overdoped BSCCO, we have found that the gap function is $\Delta(\theta) = 17.75[\cos(4\theta) + 0.46]\text{meV}$ for $T_c = 90\text{K}$, and $\Delta(\theta) = 18[\cos(4\theta) + 0.33]\text{meV}$ for $T_c = 86\text{K}$. Then we have $\Delta_s = 6\text{--}8\text{meV}$, which is not small compared with the g-wave component $\Delta_g = 18\text{meV}$. Since $\eta_4 \ll \eta_0$ (Klemm *et al.* 1998), the dominant contribution to the I_c should be the s-wave component, as observed (Li *et al.* 1999). From the magnitude of the s-wave component, we can calculate $I_c R_N = (\pi/2e)\Delta_s = 9\text{--}12\text{meV}$. The measured $I_c R_N$ value is about 8mV (Li *et al.* 1999). This is in quantitative agreement with the predicted value, considering the fact that the strong coupling effect can reduce the $I_c R_N$ value by more than 20%.

Another reliable phase-sensitive experiment is the c -axis $\text{Pb}/\text{YBa}_2\text{Cu}_3\text{O}_{7-y}$ Josephson junction experiment (Sun *et al.* 1994). This junction can be described as SINS' (where S = YBCO, S' = Pb, I represents the insulating layer and N represents the normal-metal layer). Owing to a very short coherent length ξ_c along the c -axis direction, the bulk gap will be strongly depressed at the S–I interface; the depression factor is c/ξ_c (where c is the lattice constant along the c axis) (Müller 1995). From $\xi_c = \xi_{ab}/\gamma$ (where γ is the mass anisotropy parameter and equal to about 8 for optimally doped YBCO (Willemin *et al.* 1998c)), we obtain $\xi_c = 1.7\text{\AA}$ by taking $\xi_{ab} = 14\text{\AA}$. Therefore, the gap size at the S–I interface will be suppressed by a factor of about seven. Since the bulk s-wave component Δ_s in slightly overdoped YBCO is $3\text{--}5\text{meV}$ (see §3), this component at the S–I interface should be reduced to 0.4--

0.7 meV. Then the $I_c R_N$ value is calculated to be 0.93–1.27 mV, in quantitative agreement with the measured value (about 0.9 mV) (Sun *et al.* 1994).

Now we discuss another *c*-axis Josephson tunnelling experiment in which a conventional superconductor (lead) is deposited across a single twin boundary of a YBCO crystal (Kouznetsov *et al.* 1997). Because lead is an s-wave superconductor, the lead counterelectrode couples only to the s-wave component of the YBCO OP. If YBCO were predominantly d wave, any small s-wave component added to the dominant d-wave component would change sign across the twin boundary. In this case, magnetic fields parallel to the boundary would produce a local minimum in I_c at $B = 0$, in agreement with the observation (Kouznetsov *et al.* 1997). The experimental results thus provide evidence for mixed d- and s-wave pairing symmetry in YBCO near the twin boundary with a reversal in the sign of the s-wave component across the boundary. However, if the bulk OP symmetry in a single domain were also $d + s$ or $d - s$, one would expect a nearly zero I_c in heavily twinned crystals. The fact that the observed $I_c R_N$ in heavily twinned crystals (Sun *et al.* 1994) is nearly the same as that in the single-domain crystal rules out the bulk $(d + s)$ - or $(d - s)$ -wave OP symmetry in YBCO. Therefore the only possibility is that the OP near the twin boundary rather than in the bulk is the $d + s$ or $d - s$ wave, and/or that half-flux is always trapped in the twin boundary. Theoretically it has been demonstrated that the bulk g-wave component could be changed into d-wave component near the interface (Shevchenko and Sushkov 1998). As shown above, the dominant component of the bulk OP in YBCO is the g wave, which could be changed into the d wave near the boundary.

3.6. Phase-sensitive experiments along CuO_2 planes

The phase-sensitive tricrystal experiments on both hole- and electron-doped cuprates (Tsuei and Kirtley 2000, Tsuei *et al.* 1995, 1996) show that the OP symmetry is the d wave, in contradiction with the above conclusion drawn from many bulk-sensitive experiments. In order to resolve the discrepancy, it should be noted that the tricrystal experiments are rather surface sensitive, so these experiments are probing the OP symmetry at the surface or interface, rather than in the bulk. Based on the Ginzburg–Landau free energy, Bahcall (1996) has shown that the OP symmetry near surfaces or interfaces can be different from that in the bulk if the bulk OP is strongly suppressed at the surfaces. Experimentally, the observed $I_c R_N$ values in all the tricrystal experiments are about two orders of magnitude smaller than the intrinsic Ambegaokar–Baratoff limit. For example, in the optimally doped YBCO, the magnitude of the maximum gap $\Delta_M(0)$ is about 30 meV (Ponomarev *et al.* 1996, Wei *et al.* 1998). Then the intrinsic $I_c R_N$ value should be equal to the Ambegaokar–Baratoff limit $\pi\Delta_M(0)/2e = 47$ mV, which has been confirmed by a nearly ideal SIS break junction experiment (Ponomarev *et al.* 1996). However, the observed $I_c R_N$ values in the tricrystal experiments on YBCO and $\text{Tl}_2\text{Ba}_2\text{CuO}_{6+y}$ (Tsuei *et al.* 1995, 1996) are about 1.8 and 0.5 mV respectively. These values are about two orders of magnitude smaller than the intrinsic bulk values. Similarly, the observed $I_c R_N$ value in the NCCO and PCCO tricrystal experiments is about 0.1 mV, as inferred from the measured critical current density $J_c = 6 \text{ A cm}^{-2}$ (Tsuei and Kirtley 2000) and the empirical relation between $I_c R_N$ and J_c (Kleefisch *et al.* 1998). This $I_c R_N$ value is also about two orders of magnitude smaller than the intrinsic bulk value, which is estimated to be about 8 mV with $\Delta_M(0) = 2.5T_c$ (Stadlober *et al.* 1995). Therefore, the OP at the interfaces of the grain-boundary

junctions must be strongly depressed in order to explain such small $I_c R_N$ values. This strong depression in the OP ensures the condition under which the OP symmetry near surfaces or interfaces can be different from that in the bulk (Bahcall 1996). Hence, it is very likely that the tricrystal experiments are detecting the OP symmetry at the degraded interfaces, which may be different from the intrinsic one in the bulk.

There is another way to explain the tricrystal experiments. It was shown that the interfaces of the grain-boundary junctions are intrinsically underdoped (Mannhart and Hilgenkamp 1999). For underdoped cuprates, the superconductivity mainly arises from the Bose–Einstein condensation of preformed pairs (Alexandrov 1998). In this case, the symmetry of the superconducting condensate is different from the pairing symmetry (Alexandrov 1998). The former is d-wave type while the latter is s-wave type (Alexandrov 1998). Since Josephson tunnelling probes the symmetry of the superconducting condensate, the d-wave symmetry of the condensate is consistent with the tricrystal experiments.

§4. NEUTRON RESONANCE PEAK

Over the last decade, inelastic neutron scattering (INS) experiments have provided important insight into the basic physics of high-temperature superconductors. In particular, the magnetic resonance peak has been generally observed in the double-layer cuprate superconductors such as YBCO (Bourges *et al.* 1995, 1996, Fong *et al.* 1995) and BSCCO (Fong *et al.* 1999, He *et al.* 2001) with various doping levels but is not observed in the single-layer cuprates LSCO (Lake *et al.* 1999). The peak was observed in the superconducting state and at a two-dimensional wave-vector $\mathbf{Q}_{AF} = (\pi, \pi)$. The implications of these observations for the mechanism of high-temperature superconductivity are under intense debate. Prominent features in angle-resolved photoemission and optical conductivity spectra have been attributed to interactions of this bosonic mode with fermionic quasiparticles (Abanov and Chubukov 1999, Carbotte *et al.* 1999). In a more exotic approach (Demler and Zhang 1995), the INS data are explained in terms of a collective mode in the particle–particle channel whose quantum numbers are spin 1 and charge 2. This model predicts that the resonance peak energy E_r is proportional to the doping level p . Other models based on a spin–fermion interaction also show that E_r increases with increasing p (Abanov and Chubukov 1999, Morr and Pines 1998, Brinckmann and Lee 1999). All these models are difficult to explain the very recent INS experiments on overdoped BSCCO ($T_c = 83$ K) (He *et al.* 2001). The experiments have clearly demonstrated that E_r does not continue to increase towards overdoping but is nearly proportional to T_c (He *et al.* 2001). Qualitatively, this important experimental observation can be explained by a simple particle–hole excitation across the d-wave superconducting gap (Fong *et al.* 1995, Yin *et al.* 1997), which in turn should be proportional to T_c , at least in the overdoped range.

Here we present quantitative explanations for the neutron resonance peak and the spin gap observed in YBCO and BSCCO based on the extended s-wave OP symmetry in a single CuO_2 plane (see §3) and opposite signs of the OPs in the bonding and antibonding electron bands formed within Cu_2O_4 double layers (Mazin and Yakovenko 1995). In this picture, the neutron resonance peak is due to the excitation of electrons from the bonding band below the superconducting gap to the antibonding band above the superconducting gap.

We start first with a plot of the Fermi surface for slightly underdoped BSCCO with $T_c = 88$ K (figure 22). The Fermi surface shown in figure 22 was extended from a part of the Fermi surface that was determined by ARPES (White *et al.* 1996). One can see that only four electron wave-vectors at the Fermi surface are connected by the AF wave-vector \mathbf{Q}_{AF} . Each of these vectors forms an angle of θ_r with respect to the Cu—O bonding direction. Owing to spin-flip electron excitations across the superconducting gap, the neutron scattering amplitude at \mathbf{Q}_{AF} becomes significant above a threshold energy (Mazin and Yakovenko 1995)

$$E_g = 2\Delta(\theta_r). \quad (19)$$

Since magnetic scattering is odd with respect to the time reversal, the BCS coherence factor in the neutron scattering amplitude vanishes unless the gap $\Delta_{\mathbf{k}}$ has opposite signs for the electron wave-vectors \mathbf{k} and $\mathbf{k} + \mathbf{Q}_{AF}$ (Fong *et al.* 1995, Mazin and Yakovenko 1995). For an extended s-wave state, the gap function is $\Delta(\theta) = \Delta[\cos(4\theta) + s]$. It is clear that the condition $\Delta_{\mathbf{k}}\Delta_{\mathbf{k}+\mathbf{Q}_{AF}} < 0$ is not satisfied for the extended s-wave state in a single CuO_2 plane. However, if the OP has opposite signs in the bonding and antibonding electron bands formed within Cu_2O_4 double layers, the neutron scattering amplitude can be enhanced by the BCS coherence factor. This naturally explains why the resonance peak is not observed in the single-layer LSCO compound. Because of the existence of the extended van Hove singularity below the Fermi level (King *et al.* 1994), a sharp neutron resonance peak should occur at (Mazin and Yakovenko 1995)

$$E_r = \Delta(\theta_r) + \{[\Delta(\theta_r)]^2 + \xi_{\text{vH}}^2\}^{1/2}, \quad (20)$$

where ξ_{vH} is the energy of a saddle point below the Fermi level along the θ_r direction. The ARPES experiment on $\text{YBa}_2\text{Cu}_4\text{O}_8$ (Gofron *et al.* 1994) showed that the saddle points extend from $\theta = 0$ to $\pm 20^\circ$ with a sharp and large density of states lying at 20 ± 10 meV below the Fermi level. This implies that a sharp neutron resonance peak should be observed when $\theta_r < 20^\circ$. For $\theta_r > 20^\circ$, the neutron resonance peak will become broader, and its position is pushed away from the threshold energy. Since θ_r increases with a decrease in the doping level (see below), we shall expect that both E_g and E_r decrease and the resonance peak width increases as the doping level decreases. This is in qualitative agreement with experiment (Bourges *et al.* 1995).

From equations (19) and (20), it is easy to calculate E_g and E_r if one knows the gap function $\Delta(\theta)$ and the θ_r value. From the measured Fermi surface, one can readily determine θ_r . For example, we find $\theta_r = 18.4^\circ$ for a slightly underdoped BSCCO from figure 22. For optimally doped YBCO, there are two Fermi-surface sheets (Schabel *et al.* 1997); so we take the average of the two Fermi surface sheets to evaluate the θ_r value, which is about 16.0° . In figure 23, we show the doping dependence of the θ_r values, which are determined from the measured Fermi surfaces (White *et al.* 1996, Schabel *et al.* 1997, Golden *et al.* 2000, Legner *et al.* 2000). The doping level p is calculated from an empirical relation $T_c = T_c^{\text{max}}[1 - 82.6(p - 0.16)^2]$, where $T_c^{\text{max}} = 93.5$ K for YBCO and 95 K for BSCCO. It is interesting to see that θ_r increases with decreasing p , as expected.

For slightly overdoped BSCCO with $T_c \approx 90$ K, the gap function is $\Delta(\theta) = 17.8[\cos(4\theta) + 0.46]$ meV. With $\theta_r = 15.6^\circ$, we obtain $\Delta(\theta_r) = 16.4$ meV and $E_g = 32.8$ meV. For BSCCO, tunnelling spectra (Suzuki *et al.* 1999b) show double-peak features slightly above T_c ; one peak feature is related to a pseudogap Δ_p of about 20 meV, and the other to the van Hove singularity at $(\Delta_p^2 + \xi_{\text{vH}}^2)^{1/2} = 30$ meV.

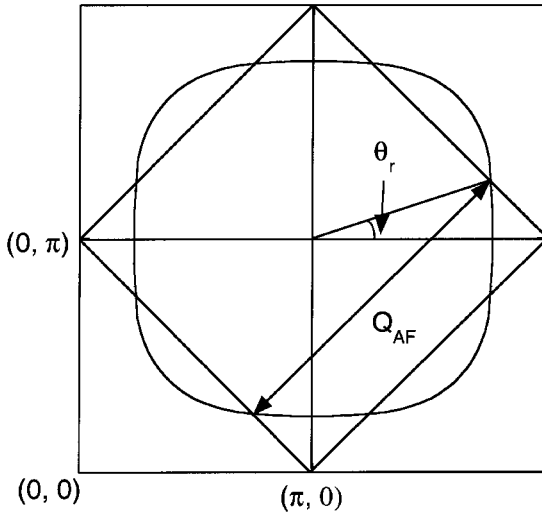


Figure 22. The Fermi surface for slightly underdoped BSCCO with $T_c = 88$ K. This Fermi surface is extended from a part of the Fermi surface that was determined by the ARPES studies (White *et al.* 1996).

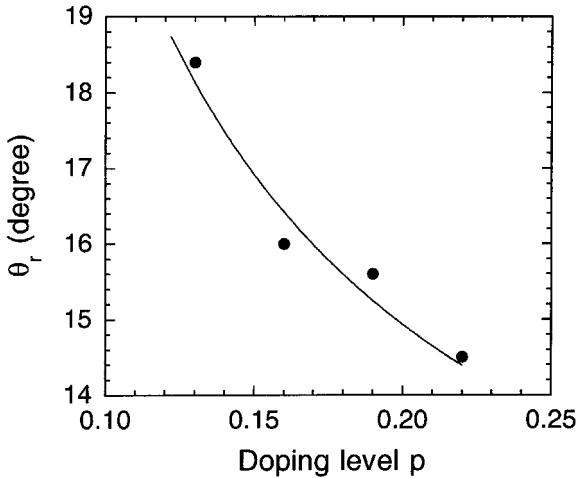


Figure 23. The doping dependence of the θ_r values, which are determined from the measured Fermi surfaces (White *et al.* 1996, Schabel *et al.* 1997, Golden *et al.* 2000, Legner *et al.* 2000). The doping level p is calculated from an empirical relation $T_c/T_c^{\max} = 1 - 82.6(p - 0.16)^2$, where $T_c^{\max} = 93.5$ K for YBCO and 95 K for BSCCO.

From this result, we obtain $\xi_{\text{vH}} = 22$ meV. With $\xi_{\text{vH}} = 22$ meV, we calculate $E_r = 43.8$ meV. The measured E_r value for a slightly overdoped BSCCO crystal ($T_c = 91$ K) is 43 ± 3 meV (Fong *et al.* 1999). As discussed above, the Raman spectra of the B_{1g} symmetry should show a peak future at the Raman shift of $2(\Delta_M^2 + \xi_{\text{vH}}^2)^{1/2}$. Using $\Delta_M = 26$ meV and $\xi_{\text{vH}} = 22$ meV, we find the peak position

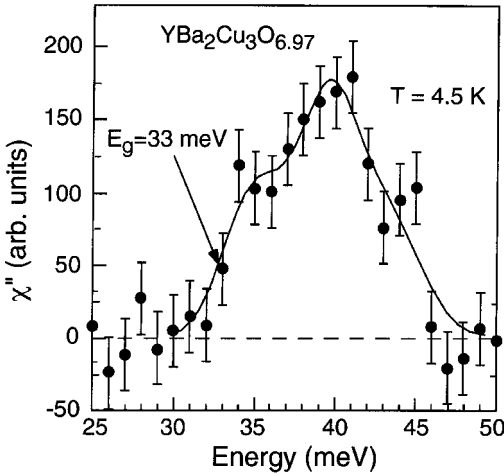


Figure 24. The imaginary part of dynamical spin susceptibility as a function of excitation energy for $\text{YBa}_2\text{Cu}_3\text{O}_{6.97}$. The figure was reproduced from the paper by Bourges *et al.* (1996).

at about 68 meV, in good agreement with the experimental result (about 66 meV) (Kendziora, Kelley and Onellion 1996).

The gap function for slightly overdoped YBCO is given by $\Delta(\theta) = 24.5 [\cos(4\theta) + 0.225]$ meV (see above). Substituting $\theta_r = 16^\circ$ into the gap function, we obtain $\Delta(\theta_r) = 16.3$ meV. In addition, the Raman spectrum of the B_{1g} symmetry in YBCO shows a sharp peak future at the Raman shift of about 65–70 meV (Cooper *et al.* 1988). Using $2(\Delta_M^2 + \xi_{vH}^2)^{1/2} = 65$ meV and $\Delta_M = 30$ meV, we obtain $\xi_{vH} = 18$ meV. Then we calculate $E_g = 32.6$ meV and $E_r = 40.6$ meV. In figure 24, we plot the imaginary part of dynamical spin susceptibility as a function of excitation energy for $\text{YBa}_2\text{Cu}_3\text{O}_{6.97}$. The figure was reproduced from the paper by Bourges *et al.* (1996). It is apparent that the calculated values for both E_g and E_r are in quantitative agreement with the experimental result shown in figure 24.

§ 5. PAIRING INTERACTION

In conventional phonon-mediated superconductors, the glue which binds two electrons or holes into the Cooper pair is the lattice deformation which provides an effective attractive force. The lattice deformation is not the only mechanism providing the microscopic attractive interaction between two charge carriers. Owing to high- T_c superconductivity and a very small isotope effect in optimally doped cuprates, many theorists have turned their minds towards an alternative glue of a purely electronic origin. The original idea that electrons themselves can be attracted to each other stems from the work of Little (1964) and Ginzburg (1968), who argued that, under certain conditions, localized electrons could change the repulsive Coulomb interaction between mobile carriers into an effective attraction. Kohn and Luttinger (1965) applied the BCS theory to fermions repelling each other at a short distance and came to the conclusion that two fermions can form non-spherical (e.g. d-wave) Cooper pairs at very low temperatures. This was possibly owing to the screening effect from other fermions, as discovered earlier by Friedel

(1954). Based on the fact that many high- T_c materials have their AF insulating counterparts such as La_2CuO_4 , Schrieffer *et al.* (1989) identified magnetic polarons (spin bags) as the source of the pairing mechanism. Millis *et al.* (1990) argued that the magnetic interaction between carriers due to AF fluctuations could explain the high- T_c and the anomalous normal-state properties in cuprates. In a more exotic theory, Anderson (1998) proposed that a very strong electron–electron repulsion could lead to charge and spin separation and to high- T_c superconductivity.

At present, no consensus has been reached concerning the pairing interactions in the high- T_c cuprates. Since the parent insulating compounds are AF, it is natural to expect that the AF fluctuations should play a significant role in the pairing. On the other hand, the large and unconventional isotope effects observed in cuprates (see §2) suggest that the electron–phonon interactions should be seriously taken into account in the description of the basic physics of cuprates.

There are several important facts which appear not to indicate that the AF fluctuations are important in bringing about high-temperature superconductivity. First, T_c does not correlate with the magnetic scattering intensity; the magnetic scattering in $\text{YBa}_2\text{Cu}_3\text{O}_7$ is significantly reduced compared with that in $\text{YBa}_2\text{Cu}_3\text{O}_{6.92}$ while the T_c values of the two compounds are similar (Bourges 1998). Secondly, there is negligible magnetic scattering in the normal state (300 K) below 30 meV in $\text{YBa}_2\text{Cu}_3\text{O}_{6.95}$ corresponding to about 3.2% of the copper atoms carrying a spin $\frac{1}{2}$ (Smith *et al.* 1998). Thirdly, the pairing symmetry is of an extended s-wave type in hole-doped cuprates and an anisotropic s-wave type in electron-doped cuprates, in contrast with the pure d-wave state predicted by the magnetic fluctuation scenario.

Moreover, the recent neutron scattering and ARPES experiments place even more serious constraints on the role of the spin fluctuations. Based on the spin–fermion model, Abanov and Chubukov (1999) have demonstrated that the neutron magnetic resonance peak and the peak, dip and hump features observed in angle-resolved photoemission spectra are due to feedback effects on the damping of spin fluctuations in a d-wave superconductor. The model predicts that the resonance peak energy E_r is inversely proportional to the spin correlation length, and thus increases with increasing doping level p . Another important prediction is that E_r exactly equals the peak–dip separation $E_{\text{dip}} - E_{\text{pk}}$ in the angle-resolved photoemission spectra. Indeed, the INS and ARPES experiments on slightly overdoped BSCCO are in quantitative agreement with the theoretical prediction, namely $E_r \approx E_{\text{dip}} - E_{\text{pk}}$ in this particular compound. However, a very recent neutron experiment on overdoped BSCCO ($T_c = 83$ K) (He *et al.* 2001) does not support the theoretical prediction; E_r does not continue to increase towards overdoping but is proportional to T_c . In figure 25, we plot the dependence of E_r on T_c . In the underdoped range, the theory is in qualitative agreement with the experimental results, while the disagreement becomes apparent in the overdoped range.

Recently, the angle-resolved photoemission spectra have become available for BSCCO with various doping levels. In figure 26, we reproduce the angle-resolved photoemission spectra for BSCCO from the paper by Ding *et al.* (2000). We select some spectra with well-defined peak and dip features to determine the values of $E_{\text{dip}} - E_{\text{pk}}$. In figure 27, we show $E_{\text{dip}} - E_{\text{pk}}$ as a function of T_c . The value of $E_{\text{dip}} - E_{\text{pk}}$ for heavily overdoped BSCCO ($T_c = 60$ K) is obtained from an angle-resolved photoemission spectrum in the paper by Vobornik *et al.* (1999). We can see that the separation $E_{\text{dip}} - E_{\text{pk}}$ is nearly independent of T_c or the doping level p . This

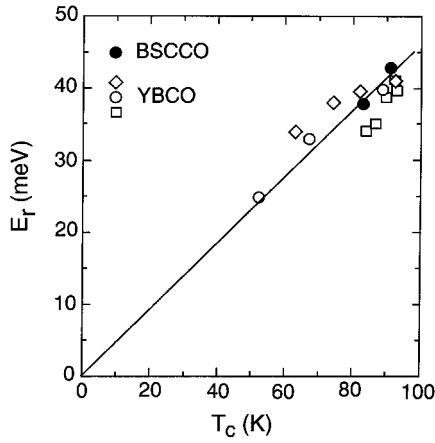


Figure 25. The dependence of the neutron resonance peak energy E_r as a function of T_c : (\diamond), (\circ), (\square), results for YBCO obtained by three independent groups. (After He *et al.* (2001).)

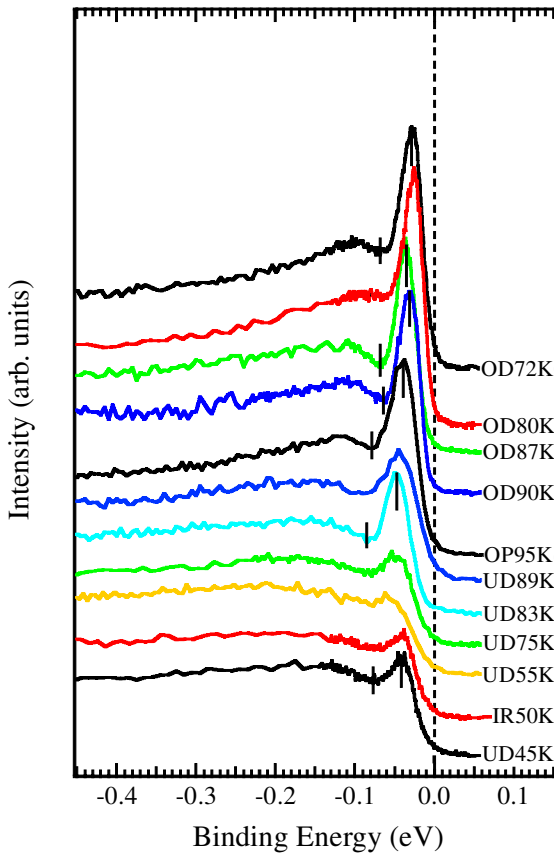


Figure 26. The angle-resolved photoemission spectra for BSCCO with different doping levels. The vertical lines mark the positions of some well-defined peak and dip features. For example, the label OD72K represents an overdoped sample with $T_c = 72$ K. (After Ding *et al.* (2000).)

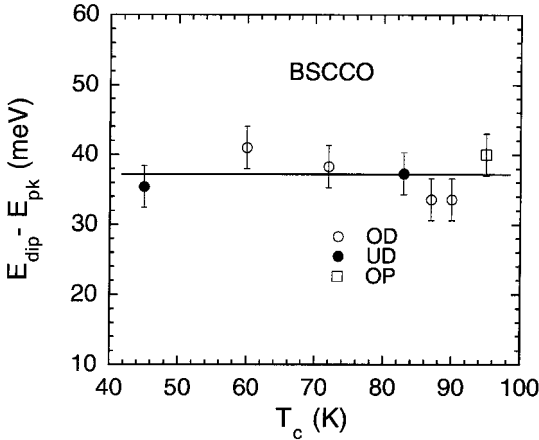


Figure 27. $E_{\text{dip}} - E_{\text{pk}}$ as a function of T_c , as determined from some spectra (indicated by vertical lines) in figure 26. The value of $E_{\text{dip}} - E_{\text{pk}}$ for heavily overdoped BSCCO ($T_c = 60$ K) is obtained from an angle-resolved photoemission spectrum published by Vobornik *et al.* (1999).

is in sharp contrast with the resonance peak energy E_r which is approximately proportional to T_c . Therefore, from figures 25 and 27, we can conclude that E_r is not equal to $E_{\text{dip}} - E_{\text{pk}}$. This is in serious contradiction with the theoretical prediction based on a strong interaction between spin fluctuations and charge carriers (Abanov and Chubukov 1999). In fact, we have shown that E_r is related to the particle-hole excitations across the superconducting gap (see §4). The dip feature in the angle-resolved photoemission spectra can be well explained by a strong interaction between charge carriers and bosonic excitations (presumably phonons) with an energy of about 20 meV (Wernbter and Tewordt 1992). Below we shall further show that, in the 90 K superconductors, the strong interaction between charge carriers and the phonons with an energy of about 20 meV is in quantitative agreement with tunnelling and optical spectra, as well as the general phonon density determined by neutron experiments and lattice dynamics calculations.

For conventional superconductors, an isotropic electron-phonon spectral density $\alpha^2 F(\omega)$, which reflects the pairing strength, can be determined from tunnelling data in the superconducting state (Carbotte 1990). In principle, information on $\alpha^2 F(\omega)$ can also be obtained through inversion of optical data although this has only been accomplished for lead. Recently, Marsiglio *et al.* (1998) introduced a dimensionless function $W(\omega)$ which is defined as the second derivative of the normal-state optical scattering rate $\tau^{-1}(\omega) = (\Omega_p^2/4\pi)\Re\sigma^{-1}(\omega)$ multiplied by frequency ω . Here Ω_p is the bare plasma frequency and $\sigma(\omega)$ the normal-state optical conductivity. Specifically,

$$W(\omega) = \frac{1}{2\pi} \frac{d^2}{d\omega^2} \frac{\omega}{\tau(\omega)}, \quad (21)$$

which follows directly from experiment, provided that the data on $\sigma(\omega)$ is sufficiently accurate that a meaningful second derivative can be taken, possibly after smoothing. Marsiglio *et al.* (1998) made the very important observation that, within the phonon range, $W(\omega) \approx \alpha^2 F(\omega)$. Beyond the phonon range, $W(\omega)$ can be negative but this

does not distract from the fact that $W(\omega)$ can be used to obtain the shape and magnitude of $\alpha^2F(\omega)$. Application of equation (21) to the normal-state conductivity of K_3C_{60} (Marsiglio *et al.* 1998) gave an $\alpha^2F(\omega)$ in excellent agreement with INS data on the phonon frequency distribution $F(\omega)$. In the superconducting state, the phonon that is strongly coupled to electrons will appear at an energy of $2\Delta + \omega_{\text{ph}}$ (where ω_{ph} is the phonon energy), that is the energies of the phonon structures shift upwards by the pair-breaking energy 2Δ .

Therefore, the electron–phonon (electron–boson) spectral density can be obtained from both optical and tunnelling data. Accurate reflection measurements at infrared wavelengths are now available for a variety of the copper oxides, which allow one to extract precisely $W(\omega) \approx \alpha^2F(\omega)$ (Carbotte *et al.* 1999, Schachinger and Carbotte 2000). On the other hand, it is difficult to obtain reliable tunnelling spectra for high-temperature superconductors owing to a short coherent length. Nevertheless, to our knowledge, there are two high-quality tunnelling spectra for slightly overdoped YBCO (Wei *et al.* 1998) and BSCCO (Gonnelli *et al.* 1997). We shall provide a coherent picture for the pairing interaction responsible for high-temperature superconductivity in cuprates by comparing the optical, tunnelling, APRES, and neutron data. These data consistently show a very strong coupling feature at $\omega_{\text{ph}} \approx 20$ meV.

In figure 28, we show normalized conductance data for scanning tunnelling microscopy on a slightly overdoped YBCO crystal with a Pt–Ir tip at 4.2 K (Wei *et al.* 1998). The crystal has $T_c \approx 90$ K with approximately 1 K transition width (Wei *et al.* 1998). The tunnelling spectrum shows a negligible zero-bias conductance and thus represents the intrinsic density of states of the CuO_2 planes in YBCO (the normal carriers near oxygen vacancies in the chains would contribute a large zero-bias conductance). It is striking that the strong-coupling features similar to that in conventional superconductors can be clearly seen in the spectrum (as indicated by the arrows). The strong-coupling features correspond to a very strong coupling between charge carriers and the phonons with $\omega_{\text{ph}} = 19$ meV. The phonon density of states in optimally doped YBCO also reveals a large peak at about 20 meV

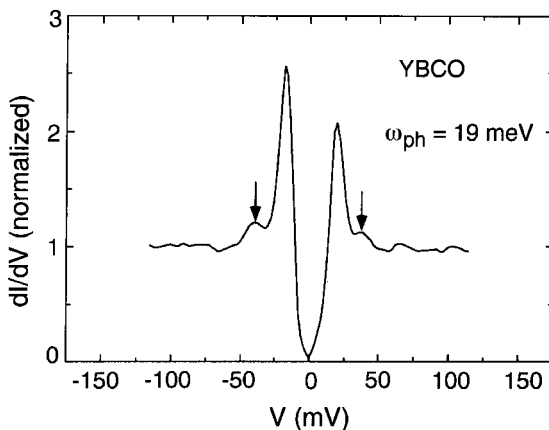


Figure 28. The normalized conductance data from scanning tunnelling microscopy on a slightly overdoped YBCO crystal with a Pt–Ir tip at 4.2 K. The strong-coupling features (indicated by arrows) at a bosonic energy of 19 meV are clearly seen in the spectrum. (After Wei *et al.* (1998).)

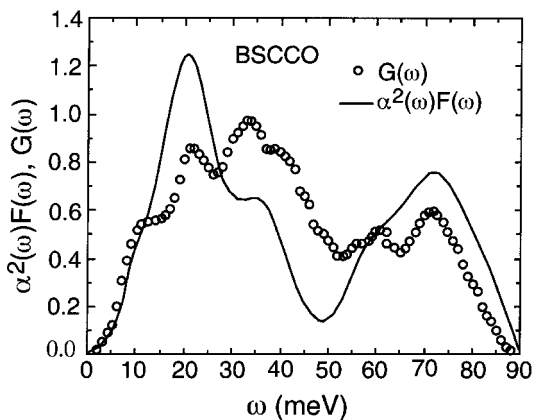


Figure 29. The electron–phonon spectral density $\alpha^2 F(\omega)$ for an optimally doped BSCCO crystal, which was deduced from an SIS break-junction spectrum (Gonnelli *et al.* 1997).

(Renker *et al.* 1988). Further, the lattice dynamics calculation (Nozaki and Itoh 1993) indicates that the large peak at 18 meV mainly comes from vibrations of the oxygen and copper atoms. Thus, the low-energy phonon mode with $\omega_{\text{ph}} = 18\text{--}19$ meV has a strong coupling with conduction electrons.

In figure 29, we plot the electron–phonon spectral density $\alpha^2 F(\omega)$ for an optimally doped BSCCO crystal, which was extracted from an SIS break-junction spectrum (Gonnelli *et al.* 1997). A strong-coupling feature at an energy of about 20 meV is clearly seen. This feature also corresponds to the large peak in the phonon density of states at about 20 meV.

As discussed above, the strong-coupling feature should also appear in the optical data, that is in $W(\omega)$. Since there are two gap features in the extended s-wave gap function of hole-doped cuprates, one should expect two peak features in $W(\omega)$ at $2\Delta_M + \omega_{\text{ph}}$ and at $2\Delta_D + \omega_{\text{ph}}$. For optimally doped YBCO, $\Delta_M = 27\text{--}30$ meV and $\Delta_D = 19\text{--}21$ meV, the two peak features would be separated by about 6–11 meV,

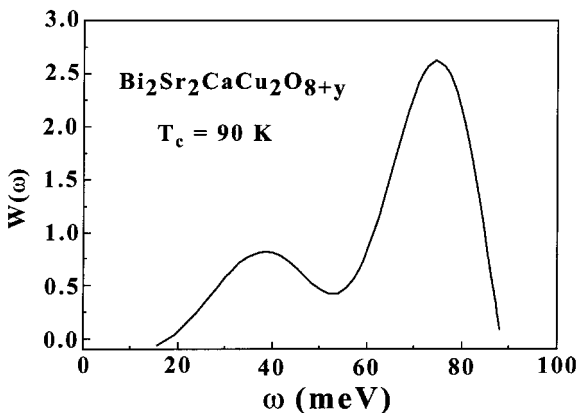


Figure 30. The optically determined electron–phonon spectral density $W(\omega)$ for a slightly overdoped BSCCO crystal with $T_c = 90$ K. (After Schachinger and Carbotte (2000).)

which is too small to be resolved. Instead, one should see a single broad peak at about $\Delta_M + \Delta_D + \omega_{\text{ph}} \approx 68 \text{ meV}$, in remarkably good agreement with the experimental result (Carbotte *et al.* 1999). For slightly overdoped BSCCO with $T_c = 90 \text{ K}$, $\Delta_M = 26\text{--}27 \text{ meV}$ and $\Delta_D = 9.5 \text{ meV}$. So one should expect two peak features in $W(\omega)$ at 38 meV and at $72\text{--}74 \text{ meV}$. This is in excellent agreement with the experimental result reproduced in figure 30 (Schachinger and Carbotte 2000). The double-peak features at about 38 meV and at 74 meV are well resolved owing to a large difference between Δ_D and Δ_M in this compound. The much larger amplitude of $W(\omega)$ along the maximum gap direction indicates a much stronger electron–phonon coupling which leads to a much larger gap. Therefore, the extended s-wave pairing symmetry and strong electron–phonon coupling at the phonon energy of about 20 meV are in quantitative agreement with tunnelling, neutron, optical and ARPES spectra.

§ 6. PAIRING THEORY

In the previous section, we have clearly demonstrated that the AF fluctuations do not play an important role in bringing about high-temperature superconductivity. In contrast, the strong electron–phonon interaction and the formation of polaronic carriers are crucial to the understanding of the physics of cuprates. A correct theory should be able to explain quantitatively the pseudogap in the normal state, the supercarrier mass anisotropy, the isotope effects, the doping and T_c dependences of the penetration depth, and some other physical properties. Here we shall attempt to explain all these properties quantitatively and consistently.

We start with the normal-state susceptibility $\chi(T)$. The temperature dependence of the normal-state susceptibility in cuprates is very different from that in conventional metals. It was found (Johnston 1989) that $\chi(T)$ exhibits a broad peak at a temperature T_{max} . Such behaviour was interpreted in terms of the two-dimensional AF correlation between copper spins. However, Nakano *et al.* (1994) have shown that, at low temperatures, $\chi(T)$ strongly deviates from the prediction of the two-dimensional AF model. Furthermore, the magnitude of $\chi(T)$ is proportional to the electronic specific heat (Loram *et al.* 1996), implying that $\chi(T)$ reflects the density of states of the conduction electrons rather than the localized spin correlation. Alternatively, Alexandrov *et al.* (1996) explained the normal-state susceptibility data on the basis of their small-(bi)polaron theory which predicts a temperature-dependent spin susceptibility: $\chi_{\text{AKM}}(T) = B_\infty T^{-1/2} \exp(-\Delta_{\text{bp}}/2T)$, where Δ_{bp} is the bipolaron binding energy and B_∞ is a constant depending on the effective masses of polarons and bipolarons (Alexandrov *et al.* 1996). If we consider a possible coexistence of Fermi-liquid-type carriers and (bi)polarons, the total susceptibility for the two-component system is $\chi(T) = f_s \chi_{\text{AKM}}(T) + (1 - f_s) \chi_{\text{F}} + \chi_{\text{cV}}$. Here f_s is the fraction of the domains (in momentum or real space) occupied by the (bi)polaronic carriers, χ_{F} is the susceptibility contributed from the Fermi-liquid-type carriers and χ_{cV} is the total orbital contribution. Then

$$\chi(T) = f_s B_\infty T^{-1/2} \exp\left(-\frac{\Delta_{\text{bp}}}{2T}\right) + \chi_0. \quad (22)$$

Figure 31 shows the temperature dependence of the normal-state susceptibility for LSCO. For $x = 0.20$, a small Curie paramagnetic susceptibility has been subtracted. The horizontal line indicates the total orbital contribution, as determined from the ^{63}Cu Knight shift (Song *et al.* 1993). The solid curves in figure 31 represent

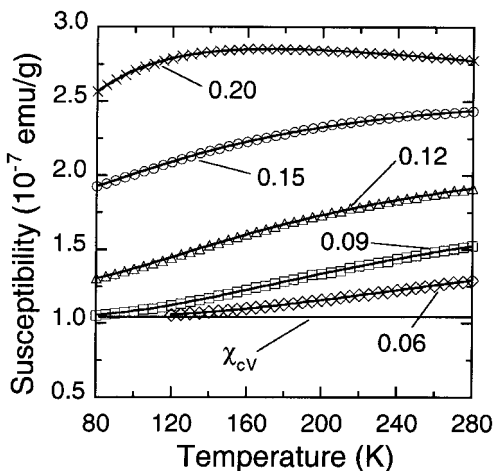


Figure 31. The temperature dependence of the normal-state susceptibility for LSCO (Reproduced from the paper by Müller *et al.* (1998).) The total orbital contribution χ_{cv} is indicated by a horizontal line, as determined from the ^{63}Cu Knight shift (Song *et al.* 1993).

the fitting curves using equation (22). The fitting is excellent for all the compositions. It is interesting to see that, for $x > 0.09$, $(1 - f_s)\chi_F \neq 0$, that is the Fermi-liquid-type carriers set in. From the more extended $\chi(T)$ data (Loram *et al.* 1996), one sees that, for $x \leq 0.10$, only (bi)polaronic charge carriers exist, and that the fraction of the Fermi-liquid carriers increases monotonically with x for $x > 0.10$. Therefore, the theory of bipolaronic superconductivity should be applied for $x \leq 0.10$.

Figure 32 shows the composition dependences of the bipolaron binding energy Δ_{bp} and $E_m/2 \equiv g^2\hbar\omega$. Here E_m is an energy corresponding to the maximum ac conductivity in the mid-infrared region (Bi and Eklund 1993), ω is the characteristic optical phonon frequency and g^2 is related to the polaron mass enhancement factor

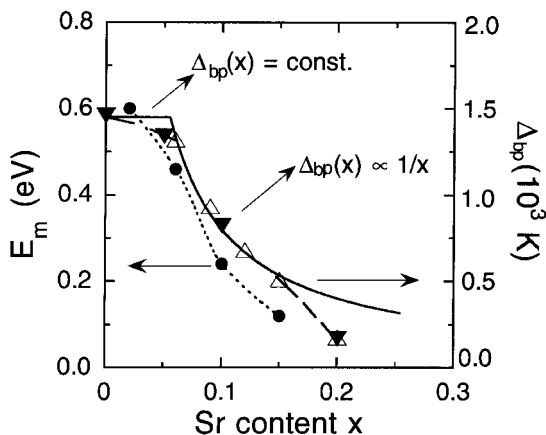


Figure 32. The strontium content dependences of the bipolaron binding energy Δ_{bp} and $E_m/2 \equiv g^2\hbar\omega$ for LSCO. (Reproduced from the paper by Müller *et al.* (1998).) Here E_m is an energy corresponding to the maximum ac conductivity in the mid-infrared region (Bi and Eklund 1993).

$\exp(g^2)$. Since $T_{\max} = \Delta_{\text{bp}}$ according to equation (22), we include T_{\max} values (open triangles) as determined by Johnston (1989). In fact, the data in the paper of Johnston (1989) can be excellently fitted by equation (22) over a wide temperature region (50–800 K) (Müller *et al.* 1998). From the figure, one can also see that Δ_{bp} is proportional to $1/x$ ($\Delta_{\text{bp}} = 6.9 \text{ meV}/x$) for $0.06 \leq x \leq 0.15$; below $x = 0.05$, Δ_{bp} is nearly doping independent; above $x = 0.15$, Δ_{bp} decreases more rapidly. All these features are predicted by the theory of Alexandrov *et al.* (1996). Furthermore, the magnitude of Δ_{bp} is about 44 meV for $x = 0.15$, in excellent agreement with the *c*-axis optical conductivity which starts to decrease below about 45 meV (Uchida 1997). This provides compelling evidence that the pseudogap deduced from the susceptibility data is the charge gap rather than the spin gap.

Now a question arises about the physical origin of the two components. As we know that the parent insulating cuprates are charge-transfer insulators, so doped holes mainly reside on the oxygen orbitals as long as the charge-transfer gap is larger than a critical value. The doped oxygen holes can form polarons and bipolarons owing to a strong electron–phonon interaction (Alexandrov and Mott 1995). This should be the case for $x \leq 0.10$, as schematically depicted in figure 33(a). Such an electronic structure can be constructed from the constrained ‘local-density approximation + U ’ calculation. When the doping level increases, the charge-transfer gap gradually decreases (Raimondi *et al.* 1993). Above a critical doping level, the charge-transfer gap becomes small enough to form a single band which should be similar to that predicted by slave-boson calculations that take into account a strong electron–electron correlation on the copper sites (see the review article by Markiewicz (1997)). This should happen for $x > 0.25$, as plotted in figure 33(b). For $0.10 < x < 0.25$, it is natural to expect an inhomogeneous electronic state which might be a linear combi-

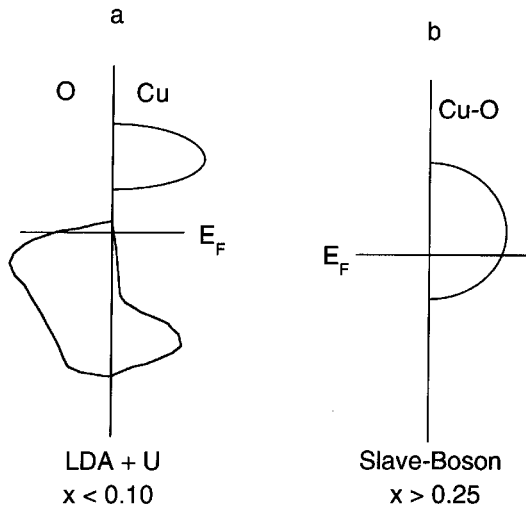


Figure 33. The schematic electronic structures for hole-doped cuprates. For $x \leq 0.10$, the electronic structure is consistent with a doped charge-transfer insulator and can be constructed from the local-density approximation + U method. Doped holes mainly reside on the oxygen orbitals. For $x > 0.25$, the electronic structure is in agreement with the prediction of the slave-boson calculation which has taken into account a strong correlation effect.

nation of the two stable electronic structures shown in figures 33(a) and (b). This could explain the coexistence of two types of charge carrier implied by the normal-state susceptibility data.

The above scenario also points towards a large Fermi surface for $x > 0.10$ and small hole pockets for $x \leq 0.10$ in LSCO. The critical doping level for such a cross-over may differ from system to system. Since the fraction of the electronic structure of figure 33(b) (corresponding to a large Fermi surface) increases with increasing doping level x , the photoemission intensity will increase with increasing x . All these features are consistent with experiment (Markiewicz 1997). Furthermore, this picture is in quantitative agreement with the doping dependences of the carrier density n and the bare plasma frequency $\hbar\Omega_p (\propto (n/m_b)^{1/2})$, as shown in figures 34 and 35. From figure 34, one can see that the residual sheet resistance at 1% Zn doping is consistent

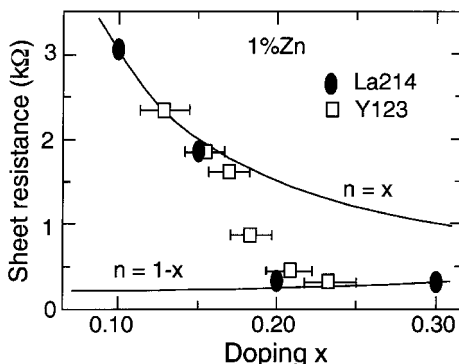


Figure 34. The residual sheet resistance at 1% Zn doping for doped LSCO and YBCO. (After Fukuzumi *et al.* (1996).)

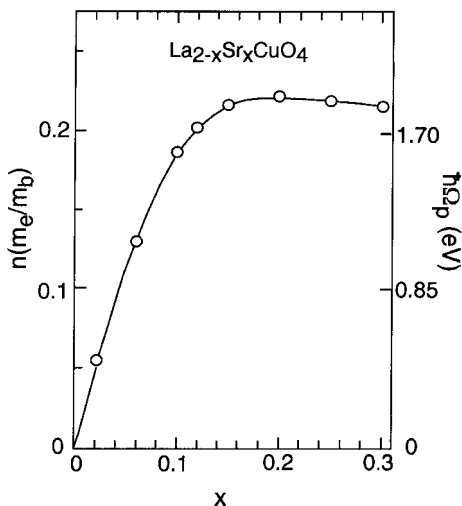


Figure 35. The doping dependence of the bare plasma frequency $\hbar\Omega_p (\propto (n/m_b)^{1/2})$ in LSCO. (After Tamasaku *et al.* (1994).)

with the fact that $n = x$ for $x < 0.15$, and $n = 1 - x$ for $x > 0.25$. Because of the experimental uncertainty, it is likely that $n = x$ holds only for $x \leq 0.10$. This is in agreement with the result shown in figure 35 where we can see clearly that $n \approx x$ with $m_b \approx 0.5m_e$ for $x \leq 0.10$ (where m_e is the electron mass). From the deduced m_b , we can calculate the bare hopping integral $t_{ab} = \hbar^2/2a^2m_b = 0.5$ eV. This value is just equal to the geometric average of the calculated bare hopping integrals $t_{pp\sigma}$ and $t_{pp\pi}$ for the oxygen orbitals ($t_{pp\sigma} = 0.87$ eV and $t_{pp\pi} = -0.26$ eV (McMahan *et al.* 1988)). This consistency justifies the electronic structure shown in figure 33 (a). Owing to a large anisotropy in the hopping integrals, the oxygen bands are almost one dimensional. Further, the polaronic mass enhancement factor could be larger along the directions with a much smaller hopping integral (Kornilovitch 1999). This will increase the anisotropy further so that the oxygen polaron bands become more one-dimensional like, in agreement with the observation of the extended van Hove singularity (Dessau *et al.* 1993, Gofron *et al.* 1994). The measured band dispersion for the slightly overdoped BSCCO can be best described by a sum of the one-dimensional-like oxygen bands and the band predicted by slave-boson calculations. Because of the interaction between the two types of carrier, we may still consider it as a single band when we discuss the low-energy physics.

For $x > 0.25$, the band dispersion is similar to that calculated from the slave-boson method. The predicted bandwidth from the slave-boson calculation (Markiewicz 1997) is nearly the same as that determined from the ARPES studies (Dessau *et al.* 1993). Furthermore, the calculated plasma frequency $\hbar\Omega_p$ is about 1.7 eV for $x = 0.3$ (Markiewicz 1997), in remarkably good agreement with the measured value (1.8 eV) for $x = 0.3$ (see figure 35).

Now we turn to discussion on the electron–phonon interaction in doped cuprates. Perhaps the most intriguing experimental evidence of a large and anomalous electron–lattice interaction comes from INS experiments on various high-temperature superconducting materials (Pintschovius and Reichardt 1994, McQueeney *et al.* 1999, Petrov *et al.* 2000). These experiments clearly show that the Cu–O bond stretching mode in the CuO_2 planes is very strongly coupled to the doped holes. The average frequency of this mode is about 75 meV in $\text{La}_{1.85}\text{Sr}_{0.15}\text{CuO}_4$ (McQueeney *et al.* 1999), and about 60 meV in $\text{YBa}_2\text{Cu}_3\text{O}_{6.92}$ (Petrov *et al.* 2000). The infrared spectra of the oxygen-isotope-exchanged YBCO indicate that the frequency of this mode shifts down by about 4% upon replacing ^{16}O with ^{18}O (Crawford *et al.* 1988). The result is in good agreement with a theoretical calculation (Henn *et al.* 1997). Therefore the Cu–O stretching mode, which is related to vibrations of both oxygen and copper atoms in the CuO_2 planes (Henn *et al.* 1997), may play an important role in the physics of cuprates.

The strong coupling of the stretching mode with doped holes may lead to the formation of polarons and bipolarons. In the theory of bipolaronic superconductivity, Alexandrov and Mott (1995) considered apical-oxygen hole polarons and bipolarons. However, we believe that the in-plane oxygen holes form polarons and bipolarons since doped holes are mainly from the in-plane oxygen orbitals (Pellegrin *et al.* 1993). In this case, we might expect that the effective mass of the intersite bipolaron is approximately twice the polaron mass. We shall see that this scenario is able to explain quantitatively several physical properties such as the doping dependences of the isotope effects, the supercarrier mass anisotropy, and the penetration depth in the doping region of $x \leq 0.10$ where nearly all the charge carriers are (bi)polarons.

As discussed above, the effective hopping integral for intersite bipolarons in the CuO_2 plane is

$$t_{ab}^{**} \approx 0.5t_{ab} \exp(-g^2). \quad (23)$$

Along the c axis, the intersite bipolaron behaves like the on-site bipolaron whose effective mass is strongly enhanced (Alexandrov *et al.* 1996). The hopping integral is in general written as (Alexandrov and Mott 1995)

$$t_c^{**} = \frac{2t_c^2}{A_{\text{bp}}} \exp(-2g^2) \sum_{k=0}^{\infty} \frac{(-2g^2)^k}{k!(1+k\hbar\omega/A_{\text{bp}})}. \quad (24)$$

In the case when $\hbar\omega < A_{\text{bp}} < 2g^2\hbar\omega$, one has

$$t_c^{**} = 2t_c^2 \left(\frac{2\pi}{\hbar\omega A_{\text{bp}}} \right)^{1/2} \exp \left\{ -2g^2 - \frac{A_{\text{bp}}}{\hbar\omega} \left[1 + \ln \left(\frac{2g^2\hbar\omega}{A_{\text{bp}}} \right) \right] \right\}. \quad (25)$$

From this equation, one readily sees that t_c^{**} decreases rapidly with increasing A_{bp} and g^2 . Using $m_{ab}^{**} = \hbar^2/2a^2 t_{ab}^{**}$ and $m_c^{**} = \hbar^2/2d^2 t_c^{**}$ (where d is the interlayer distance), we define the supercarrier mass anisotropy $\gamma = (m_c^{**}/m_{ab}^{**})^{1/2} = (a^2 t_{ab}^{**}/d^2 t_c^{**})^{1/2}$. Similarly, the bare mass anisotropy is $\gamma_b = (m_c/m_{ab})^{1/2} = (a^2 t_{ab}/d^2 t_c)^{1/2}$.

With $n = x$, the inplane penetration depth $\lambda_{ab}(0)$ for $x \leq 0.10$ is given by

$$\lambda_{ab}(0) = \left(\frac{d\hbar^2 c^2 \exp(g^2)}{8\pi e^2 x t_{ab}} \right)^{1/2}. \quad (26)$$

From figure 32, we have determined that $A_{\text{bp}} = 6.9 \text{ meV}/x$, $g^2 \approx 0.180/x$ for ^{16}O and $g^2 \approx 0.187/x$ for ^{18}O . Here we have taken $\hbar\omega = 75.0 \text{ meV}$ for ^{16}O and 72.1 meV for ^{18}O (see the above discussion). We also know that $\gamma_b \approx 5$ (Allen *et al.* 1987) and $t_{ab} = 0.5 \text{ eV}$. With these unbiased parameters and using equations (23), (24) and (26), we can calculate the doping dependences of γ (for both ^{16}O and ^{18}O), of $\Delta m_{ab}^{**}/m_{ab}^{**}$, of $\Delta m_c^{**}/m_c^{**}$ and of $\lambda_{ab}(0)$. The calculated results (solid and broken curves) are shown in figure 36 together with the experimental data (full and open circles). It is remarkable that the theory is in quantitative agreement with experiment in all cases. In particular, the calculated supercarrier mass anisotropy increases rapidly with decreasing x and depends strongly on the oxygen mass at low doping levels x , in agreement with the experimental results. Thus, the experimental results in deeply underdoped cuprates strongly support the theory of bipolaronic superconductivity.

Now let us consider the physics of optimally doped and overdoped cuprates. We believe that the coexistence of the Fermi-liquid carriers (with a large Fermi surface) and the one-dimensional-like polaronic carriers (with small hole pockets) is the key for understanding the superconductivity in optimally doped and overdoped cuprates. The polaronic effects still play an essential role in bringing about high-temperature superconductivity in this doping regime. As discussed above, the phonon modes at about 20 and 70 meV are strongly coupled with doped holes. When the Fermi energy E_F in the oxygen bands is smaller than these phonon energies, the phonon-induced effective interaction between carriers is non-retarded so that the real-space pairing (e.g. intersite bipolaron formation) becomes possible. This should be the case for $x \leq 0.10$ in LSCO. In contrast, E_F may lie in between 20 and 70 meV in the high-doping regime, so that the pairing interaction becomes

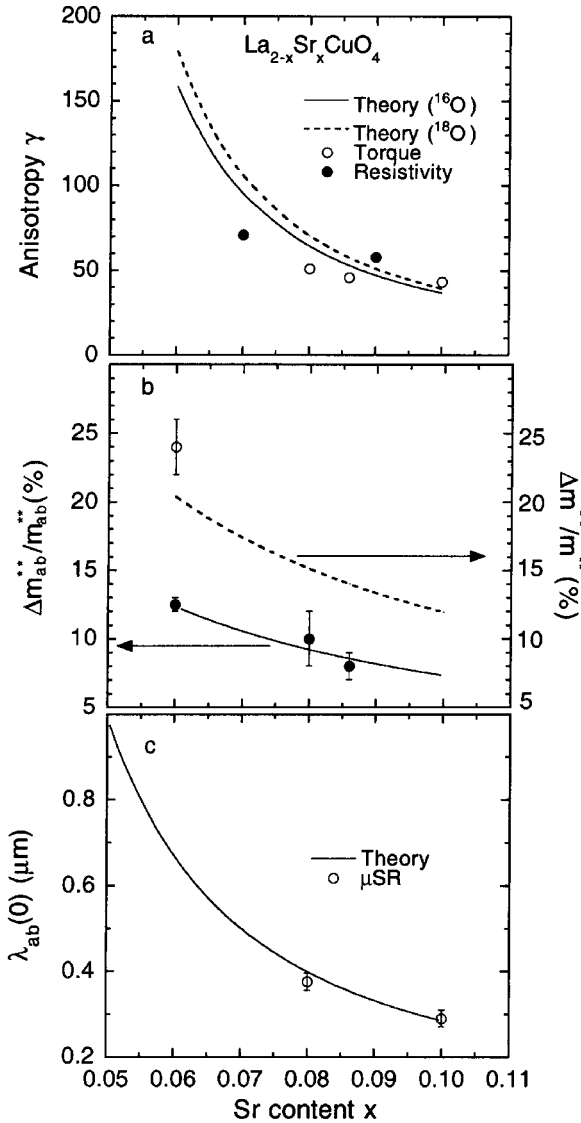


Figure 36. The calculated supercarrier mass anisotropy $\gamma \equiv (m_c^{**}/m_{ab}^{**})^{1/2}$ (for both ^{16}O and ^{18}O), $\Delta m_{ab}^{**}/m_{ab}^{**}$, $\Delta m^{**}/m^{**}$ and $\lambda_{ab}(0)$ as functions of the doping level x (—, - - - -). Here Δ means a small change upon the oxygen-isotope substitution. The experimental data (\bullet , \circ) were taken from the work of Uemura *et al.* (1989), Kimura *et al.* (1996), Zhao *et al.* (1998a), Willemin *et al.* (1999), and Hofer *et al.* (2000a,b).

retarded for low-energy phonons and remains non-retarded for high-energy phonons. The retarded electron-phonon coupling for low-energy phonons could be treated within the Migdal approximation, while the non-retarded electron-phonon coupling for high-energy phonons should be modelled separately within the polaron theory. The strong coupling between doped holes and high-energy phonons may lead to a polaronic mass enhancement and to an attractive non-retarded potential between doped holes. The polaronic holes could then form k -

space Cooper pairs by interacting with low-energy phonons. The problem could thus be solved within Eliashberg equations with an effective electron–phonon spectral density for low-energy phonons and a negative Coulomb pseudopotential produced by high-energy phonons. This approach was even applied to conventional superconductors (Carbotte 1990) where all the electron–phonon couplings are retarded. We believe that this approach should be more suitable for the present case since the Coulomb pseudopotential introduced in the Eliashberg equation is more or less non-retarded. Within this simplified approach, the effective electron–phonon coupling constant λ_{ep} for low-energy phonons is enhanced by a factor $f_p = \exp(g^2)$. The effective Coulomb pseudopotential μ^* is negative and also proportional to f_p . The effective electron–phonon spectral density $W^*(\omega)$ is equal to $W(\omega)/f_p$ since the effective plasma frequency is reduced by a factor of $f_p^{1/2}$.

For slightly overdoped BSCCO, g^2 can be evaluated from the mid-infrared optical conductivity which exhibits a maximum at $E_m \approx 0.12$ eV (Quijada *et al.* 1999). With $E_m = 0.12$ eV and $\hbar\omega = 75$ meV, we find that $g^2 = E_m/2\hbar\omega = 0.8$, leading to $f_p = 2.2$. From the result shown in figure 30, we can extract the effective electron–phonon spectral density $W^*(\omega) \approx \alpha_{\text{eff}}^2 F(\omega)$ after correcting for the polaronic mass enhancement factor. The result is plotted in figure 37. It is striking that the deduced $\alpha_{\text{eff}}^2 F(\omega)$ from the optical data is in excellent agreement with that deduced from the tunnelling spectrum (see figure 29). Using the spectral density, we calculate $\lambda_{\text{ep}} = 2.6$. If there were no polaronic mass enhancement due to high-energy phonons, the coupling constant contributed from low-energy phonons would be about 1.2. With $\mu^* = 0.1$ and $\lambda_{\text{ep}} = 1.2$, we calculate $T_c = 18$ K according to the T_c formula

$$k_B T_c = 0.25 \hbar \langle \omega^2 \rangle^{1/2} \left[\exp \left(\frac{2}{\lambda_{\text{eff}}} \right) - 1 \right]^{-1/2}, \quad (27)$$

where

$$\lambda_{\text{eff}} = \frac{\lambda_{\text{ep}} - \mu^*}{1 + 2\mu^* + \lambda_{\text{ep}}\mu^* t(\lambda_{\text{ep}})}. \quad (28)$$

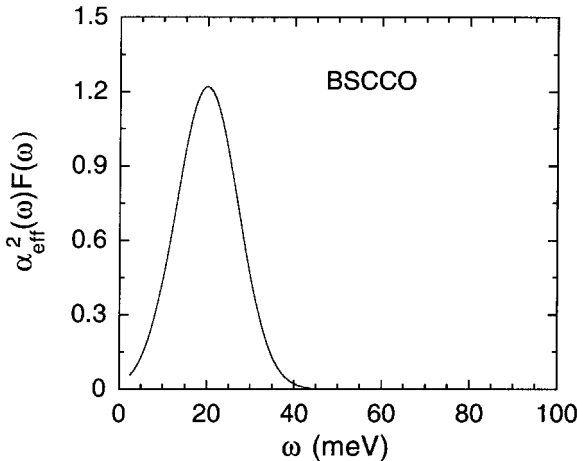


Figure 37. The effective electron–phonon spectral density $W^*(\omega) \approx \alpha_{\text{eff}}^2 F(\omega)$, which is extracted from figure 30 after correcting for the polaronic mass enhancement factor and shifting the peak position downwards by $2\Delta_M = 54$ meV.

The function $t(\lambda_{\text{ep}})$ is plotted in figure 2 of the paper by Kresin (1987). In the present case, $\hbar\langle\omega^2\rangle^{1/2}$ is contributed only from low-energy phonons and equal to 20 meV. Therefore, without high-energy phonons, T_c would not be higher than 20 K. The high-energy phonons enhance the electron–phonon coupling constant by a factor of 2.2 and cause a negative μ^* . It is also likely that the interactions of electrons with high-energy bosons of electronic origin make μ^* more negative. If we take $\mu^* = -0.14$ and $\lambda_{\text{ep}} = 2.6$, we can obtain $T_c = 91$ K. This leads to $k_B T_c / \hbar\langle\omega^2\rangle^{1/2} = 0.39$, and $2\Delta(0)/k_B T_c \approx 7$ according to the known relation between $k_B T_c / \hbar\langle\omega^2\rangle^{1/2}$ and $2\Delta(0)/k_B T_c$ (Carbotte 1990). The measured $2\Delta(0)/k_B T_c$ is indeed close to the prediction.

In terms of the above approach, we can calculate the total isotope exponent α using equations (27) and (28) as well as the relations $\lambda_{\text{ep}} \propto f_p$, $\mu^* \propto f_p$, $t(\lambda_{\text{ep}}) \approx 1.8/\lambda_{\text{ep}}$ for $\lambda_{\text{ep}} = 2-4$ (Kresin 1987). The calculated $\alpha = -0.005$. The nearly zero isotope exponent arises because the isotope dependences of λ_{ep} and μ^* due to polaronic effects cancel out the isotope effect on the pre-factor in equation (27). Therefore, the observed very small isotope effect in optimally doped 90 K superconductors is naturally explained within this picture. Moreover, the substantial isotope effect on the effective supercarrier mass even in optimally doped cuprates is also a natural consequence of the fact that polarons form Cooper pairs and condense into supercarriers.

Since Fermi-liquid carriers and polaronic oxygen holes coexist, the superconducting transition temperature of the two-component system should be modified. The detailed theoretical studies of the two-component system have been reported in a recent publication (Perali *et al.* 2000). If the superconducting transition temperature in the Fermi-liquid band is low, there will be a small mass enhancement for this type of carrier. For slightly overdoped BSCCO, the fraction of Fermi-liquid carriers may be close to 0.5. Considering that the mass enhancement factor for the oxygen holes is $f_p(1 + \lambda_{\text{ep}}) = 8$, the average mass enhancement factor for the two-component system should be about 4–5, in agreement with experiment (Quijada *et al.* 1999).

§ 7. CONCLUDING REMARKS

From previous sections, we have clearly demonstrated that the strong electron–phonon interactions play a vital role in the physics of cuprates. The strong electron–electron correlation on the copper sites of CuO_2 planes makes doped holes mainly go to the oxygen orbitals. The doped oxygen holes strongly interact with the high-energy stretching vibration modes. This interaction leads to the formation of polarons and intersite bipolarons in the underdoped region. The polarons and bipolarons are mobile because the oxygen bands are rather wide, and because a substantial on-site Coulomb repulsion prevents doped holes from forming immobile on-site bipolarons. In the high-doping region, the polarons form \mathbf{k} -space Cooper pairs and superconductivity can be explained within a modified Eliashberg theory where polaronic effects due to the interaction of doped holes with high-energy phonons must be taken into account. Therefore, high- T_c superconductivity in cuprates is a cooperative phenomenon between strong electron–electron correlation and strong electron–phonon coupling.

Interestingly, the concept of enhancing the electron–phonon coupling was the original motivation for the high- T_c discovery. Bednorz and Müller (1986) argued that there should be a strong electron–phonon interaction in perovskites with a

strong Jahn–Teller effect. Indeed, the stretching vibration mode, which is related to the Q_2 type Jahn–Teller distortion, is proved to be strongly coupled to doped holes. This high-energy Q_2 -like mode should be coupled with the low-energy tilting mode (Q_4/Q_5 -like Jahn–Teller mode) if the Cu–O–Cu bonding angle is less than 180° . Thus the low-energy phonon mode at 20 meV, which is shown to be strongly coupled to doped holes, may be the tilting mode. Both stretching and tilting modes are important to high- T_c superconductivity and to other phenomena such as charge-stripe instability. We also believe that the Q_3 -type Jahn–Teller mode does not couple strongly with doped holes. Otherwise, the bipolarons would become immobile. Indeed a strong coupling of the Q_3 -type Jahn–Teller mode with electrons in doped manganites leads to the formation of immobile bipolarons in the paramagnetic state (Zhao *et al.* 2000b). Therefore, too strong an electron–phonon interaction does not lead to high-temperature superconductivity.

ACKNOWLEDGEMENTS

We would like to thank R. Prozorov, L. Alff, S. Kamal and W. N. Hardy for sending us their published data. We also thank K. Conder for sending us unpublished data.

REFERENCES

- ABANOV, A., and CHUBUKOV, A. V., 1999, *Phys. Rev. Lett.*, **83**, 1652.
 ALEXANDROV, A. S., 1998, *Physica C*, **305**, 46.
 ALEXANDROV, A. S., KABANOV, V. V., and MOTT, N. F., 1996, *Phys. Rev. Lett.*, **77**, 4796.
 ALEXANDROV, A. S., and MOTT, N. F., 1995, *Polarons and Bipolarons* (Singapore: World Scientific).
 ALFF, L., MEYER, S., KLEEFISCH, S., SCHOOP, U., MARX, A., SATO, N., NAITO, M., and GROSS, R., 1999, *Phys. Rev. Lett.*, **83**, 2644.
 ALLEN, P. B., PICKETT, W., and KRAKAUER, H., 1987, *Phys. Rev. B*, **36**, 3926.
 ANDERSON, P. W., 1998, *The Theory of Superconductivity in the High- T_c Cuprate Superconductors* (Princeton University Press).
 BAHCALL, S. R., 1996, *Phys. Rev. Lett.*, **76**, 3634.
 BARDEEN, J., COOPER, L. N., and SCHRIEFFER, J. R., 1957, *Phys. Rev.*, **108**, 1175.
 BATLOGG, B., CAVA, R. J., JAYARAMAN, A., VANDOVER, R. B., KOUROUKLIS, G. A., SUNSHINE, S., MURPHY, D. W., RUPP, L. W., CHEN, H. S., WHITE, A., SHORT, K. T., MUJSCE, A. M., and RIETMAN, E. A., 1987, *Phys. Rev. Lett.*, **58**, 2333.
 BEDNORZ, J. G., and MÜLLER, K. A., 1986, *Z. Phys. B*, **64**, 189.
 BHATTACHARYA, A., ZUTIC, I., VALLS, O. T., GOLDMAN, A. M., WELP, U., and VEAL, B., 1999, *Phys. Rev. Lett.*, **82**, 3132.
 BI, X. X., and EKLUND, P. C., 1993, *Phys. Rev. Lett.*, **70**, 2625.
 BIANCONI, A., BIANCONI, G., CAPRARA, S., DI CASTRO, D., OYANAGI, H., and SAINI, N. L., 2000, *J. Phys.: condens. Matter*, **12**, 10655.
 BIANCONI, A., SAINI, N. L., LANZARA, A., MISSORI, M., ROSSETTI, T., OYANAGI, H., YAMAGUCHI, H., OKA, K., and ITO, T., 1996, *Phys. Rev. Lett.*, **76**, 3412.
 BORNEMANN, H. J., MORRIS, D. E., LIU, H. B., and NARWANKAR, P. K., 1992, *Physica C*, **191**, 211.
 BOURGES, P., 1998, in *The Gap Symmetry and Fluctuations in High Temperature Superconductors*, edited by J. Bok, G. Deutscher, D. Pavuna and S. A. Wolf (New York: Plenum Press), p. 349.
 BOURGES, P., REGNAULT, L. P., SIDIS, Y., and VETTIER, C., 1996, *Phys. Rev. B*, **53**, 876.
 BOURGES, P., SIDIS, Y., HENNION, B., VILLENEUVE, R., COLLIN, G., and MARUCCO, J. F., 1995, *Physica B*, **213–214**, 48.
 BRINCKMANN, J., and LEE, P. A., 1999, *Phys. Rev. Lett.*, **82**, 2915.
 BUSCHMANN, L., BOEKHOLT, M., and GÜNTHERÖDT, G., 1992, *Physica C*, **203**, 68.
 CARBOTTE, J. P., 1990, *Rev. mod. Phys.*, **62**, 1027.

- CARBOTTE, J. P., SCHACHINGER, E., and BASOV, D. N., 1999, *Nature (London)*, **401**, 354.
- CHEN, X. K., IRWIN, J. C., TRODAHL, H. J., KIMURA, T., and KISHIO, K., 1994, *Phys. Rev. Lett.*, **73**, 3290.
- CHO, J. H., BORSA, F., JOHNSTON, D. C., and TORGESON, D. R., 1992, *Phys. Rev. B*, **46**, 3179.
- CHO, J. H., CHOU, F. C., and JOHNSTON, D. C., 1993, *Phys. Rev. Lett.*, **70**, 222.
- CONDER, K., RUSIECKI, S., and KALDIS, E., 1989, *Mater. Res. Bull.*, **24**, 581.
- COOPER, L. N., 1956, *Phys. Rev.*, **104**, 1189.
- COOPER, S. L., SLAKEY, F., KLEIN, M. V., RICE, J.P., BUKOWSKI, E. D., and GINSBERG, D. M., 1988, *Phys. Rev. B*, **38**, 11934.
- CRAWFORD, M. K., FARNETH, W. E., MCCARON III, E. M., and BORDIA, R. K., 1988, *Phys. Rev. B*, **38**, 11382.
- CRAWFORD, M. K., KUNCHUR, M. N., FARNETH, W. E., MCCARON III, E. M., and POON, S. J., 1990, *Phys. Rev. B*, **41**, 282.
- DAUNT, J. G., and MENDELSSOHN, K., 1946, *Proc. R. Soc. A*, **185**, 225.
- DEMLER, E., and ZHANG, S. C., 1995, *Phys. Rev. Lett.*, **75**, 4126.
- DESSAU, D. S., SHEN, Z. X., KING, D. M., MARSHALL, D. S., LOMBARDO, L. W., DICKINSON, P. H., LOESER, A. G., DICARLO, J., PARK, C. H., KAPITULNIK, A., and SPICER, W. E., 1993, *Phys. Rev. Lett.*, **71**, 2781.
- DEUTSCHER, G., ACHSAF, N., GOLDSCHMIDT, D., REVCOLEVSCHI, A., and VIETKINE, A., 1997, *Physica C*, **282-287**, 140.
- DEWILDE, Y., MIYAKAWA, N., GUPTASARMA, P., IAVARONE, M., OZYUZER, L., ZASADZINSKI, J. F., ROMANO, P., HINKS, D. G., KENDZIORA, C., CRABTREE, G. W., and GRAY, K. E., 1998, *Phys. Rev. Lett.*, **80**, 153.
- DING, H., CAMPUZANO, J. C., BELLMAN, A. F., YOKOYA, T., NORMAN, M. R., RANDERIA, M., TAKAHASHI, T., KATAYAMAYOSHIDA, H., MOCHIKU, T., and KADOWAKI, K., 1995, *Phys. Rev. Lett.*, **74**, 2784.
- DING, H., ENGELBRECHT, J. R., WANG, Z., CAMPUZANO, J. C., WANG, S. C., YANG, H. B., ROGAN, R., TAKAHASHI, T., KADOWAKI, K., and HINKS, D. G., 2000, cond-mat/0006143.
- EMERY, V. J., KIVELSON, S. A., and ZACHAR, O., 1997, *Phys. Rev. B*, **56**, 6120.
- FONG, H. F., BOURGES, P., SIDIS, Y., REGNAULT, L. P., IVANOV, A., GU, G. D., KOSHIZUKA, N., and KEIMER, B., 1999, *Nature (London)*, **398**, 588.
- FONG, H. F., KEIMER, B., ANDERSON, P. W., REZNIK, D., DOGAN, F., and AKSAY, I. A., 1995, *Phys. Rev. Lett.*, **75**, 316.
- FRANCK, J. P., 1994, *Physical Properties of High Temperature Superconductors IV*, edited by D. M. Ginsberg (Singapore: World Scientific), p. 189.
- FRANCK, J. P., HARKER, S., and BREWER, J. H., 1993, *Phys. Rev. Lett.*, **71**, 283.
- FRIEDEL, J., 1954, *Adv. Phys.*, **3**, 446.
- FRÖHLICH, H., 1950, *Phys. Rev.*, **79**, 845.
- FUKUZUMI, Y., MIZUHASHI, K., TAKENAKA, K., and UCHIDA, S., 1996, *Phys. Rev. Lett.*, **76**, 684.
- GINZBURG, V. L., 1968, *Contemp. Phys.*, **9**, 355.
- GIOVANNINI, B., and WEISS, L., 1978, *Solid State Commun.*, **27**, 1005.
- GOFRON, K., CAMPUZANO, J. C., ABRIKOSOV, A. A., LINDROOS, M., BANSIL, A., DING, H., KOELLING, D., and DABROWSKI, B., 1994, *Phys. Rev. Lett.*, **73**, 3302.
- GOLDEN, M. S., BORISENKO, S. V., LEGNER, S., PICHLER, T., DURR, C., KNUPFER, M., FINK, J., YANG, G., ABELL, S., REICHARDT, G., MULLER, R., and JANOWITZ, C., 2000, *Physica C*, **341**, 2099.
- GONNELLI, R. S., UMMARINO, G. A., and STEPANOV, V. A., 1997, *Physica C*, **275**, 162.
- HALBRITTER, J., 1992, *J. appl. Phys.*, **71**, 339; 1999, *Supercond. Sci. Technol.*, **12**, 883.
- HARDY, W. N., BONN, D. A., MORGAN, D. C., LIANG, R.-X., and ZHANG, K., 1993, *Phys. Rev. Lett.*, **70**, 3999.
- HE, H., SIDIS, Y., BOURGES, P., GU, G. D., IVANOV, A., KOSHIZUKA, N., LIANG, B., LIN, C. T., REGNAULT, L. P., SCHOENHERR, E., and KEIMER, B., 2001, *Phys. Rev. Lett.*, **86**, 1610.
- HEBARD, A. F., FIORY, A. T., SIEGAL, M. P., PHILLIPS, J. M., and HADDON, R. C., 1991, *Phys. Rev. B*, **44**, 9753.
- HENN, R., STRACH, T., SCHÖNHERR, E., and CARDONA, M., 1997, *Phys. Rev. B*, **55**, 3285.

- HIRSCHFELD, P. J., and GOLDENFELD, N., 1993, *Phys. Rev. B*, **48**, 4219.
- HOFER, J., CONDER, K., SASAGAWA, T., ZHAO, G. M., WILLEMIN, M., KELLER, H., and KISHIO, K., 2000a, *Phys. Rev. Lett.*, **84**, 4192.
- HOFER, J., SCHNEIDER, T., SINGER, J. M., WILLEMIN, M., KELLER, H., SASAGAWA, T., KISHIO, K., CONDER, K., and KARPINSKI, J., 2000b, *Phys. Rev. B*, **62**, 631.
- HOMES, C. C., CLAYMAN, B. P., PENG, J. L., and GREENE, R. L., 1997, *Phys. Rev. B*, **56**, 5525.
- JACOBS, T., SRIDHAR, S., LI, Q., GU, G. D., and KOSHIZUKA, N., 1995, *Phys. Rev. Lett.*, **75**, 4516.
- JOHNSTON, D. C., 1989, *Phys. Rev. Lett.*, **62**, 957.
- KAMAL, S., LIANG, R. X., HOSSEINI, A., BONN, D. A., and HARDY, W. N., 1998, *Phys. Rev. B*, **58**, R8933.
- KAMIMURA, H., 1987, *Int. J. mod. Phys. B*, **1**, 873.
- KELLEY, R. J., QUITMANN, C., ONELLION, M., BERGER, H., ALMERAS, P., and MARGARITONDO, G., 1996, *Science*, **271**, 1255.
- KENDZIORA, C., KELLEY, R. J., and ONELLION, M., 1996, *Phys. Rev. Lett.*, **77**, 727.
- KIMURA, T., MIYASAKA, S., TAKAGI, H., TAMASAKU, K., EISAKI, H., UCHIDA, S., KITAZAWA, K., HIROI, M., SERA, M., and KOBAYASHI, N., 1996, *Phys. Rev. B*, **53**, 8733.
- KING, D. M., SHEN, Z. X., DESSAU, D. S., MARSHALL, D. S., PARK, C. H., SPICER, W. E., PENG, J. L., LI, Z. Y., and GREENE, R. L., 1994, *Phys. Rev. Lett.*, **73**, 3298.
- KIRTLEY, J. R., TSUEI, C. C., and MOLER, K. A., 1999, *Science*, **285**, 1373.
- KLEEFISCH, S., ALFF, L., SCHOOP, U., MARX, A., GROSS, R., NAITO, M., and SATO, H., 1998, *Appl. Phys. Lett.*, **72**, 2888.
- KLEMM, R. A., RIECK, C. T., and SCHARNBERG, K., 1998, *Phys. Rev. B*, **58**, 1051.
- KOGAN, V. G., FANG, M. M., and MITRA, S., 1988, *Phys. Rev. B*, **38**, 11958.
- KOHN, W., and LUTTINGER, J. M., 1965, *Phys. Rev. Lett.*, **15**, 524.
- KORNILOVITCH, P. E., 1999, *Phys. Rev. B*, **59**, 13531.
- KOSZTIN, I., and LEGGETT, A. J., 1997, *Phys. Rev. Lett.*, **79**, 135.
- KOUZNETSOV, K. A., SUN, A. G., CHEN, B., KATZ, A. S., BAHCALL, S. R., CLARKE, J., DYNES, R. C., GAJEWSKI, D. A., HAN, S. H., MAPLE, M. B., GIAPINTZAKIS, J., KIM, J. T., and GINSBERG, D. M., 1997, *Phys. Rev. Lett.*, **79**, 3050.
- KRESIN, V. Z., 1987, *Phys. Lett. A*, **122**, 434.
- KUGEL, K. I., and KHOMSKI, D. I., 1980, *Soviet Phys. JETP*, **52**, 501.
- LAKE, B., AEPPLI, G., MASON, T. E., SCHRÖDER, A., MCMORROW, D. F., LEFMANN, K., ISSHIKI, M., NOHARA, M., TAKAGI, H., and HAYDEN, S. M., 1999, *Nature (London)*, **400**, 43.
- LANZARA, A., ZHAO, G. M., SAINI, N. L., BIANCONI, A., CONDER, K., KELLER, H., and MÜLLER, K. A., 1999, *J. Phys.: condens. Matter*, **11**, L541.
- LEE, S.-F., MORGAN, D. C., ORMENO, R. J., BROUN, D. M., DOYLE, R. A., WALDRAM, J. R., and KADOWAKI, K., 1996, *Phys. Rev. Lett.*, **77**, 735.
- LEGNER, S., BORISENKO, S. V., DURR, C., PICHLER, T., KNUPFER, M., GOLDEN, M. S., FINK, J., YANG, G., ABELL, S., BERGER, H., MULLER, R., JANOWITZ, C., and REICHARDT, G., 2000, *Phys. Rev. B*, **62**, 154.
- LI, Q., TSAY, Y. N., SUENAGA, M., KLEMM, R. A., GU, G. D., and KOSHIZUKA, N., 1999, *Phys. Rev. Lett.*, **83**, 4160.
- LITTLE, W. A., 1964, *Phys. Rev. A*, **134**, 1416.
- LORAM, J. W., MIRZA, K. A., COOPER, J. R., ATHANASSOPOULOU, N., and LIANG, W. Y., 1996, *Proceedings of the Anniversary HTS Workshop on Physics, Materials and Applications*, edited by B. Batlogg, C. W. Chu, M. K. Chu, D. U. Gubser, and K. A. Müller (Singapore: World Scientific), p. 341.
- MA, J., QUITMANN, C., KELLEY, R. J., MARGARITONDO, G., and ONELLION, M., 1995, *Solid St. Commun.*, **94**, 27.
- MAGGIO-APRILE, I., RENNER, CH., ERB, A., WALKER, E., and FISHER, O., 1995, *Phys. Rev. Lett.*, **75**, 2754.
- MANNHART, J., and HILGENKAMP, H., 1999, *Physica C*, **317–318**, 383.
- MARKIEWICZ, R. S., 1997, *J. Phys. Chem. Solids*, **58**, 1179.
- MARSIGLIO, F., STARTSEVA, T., and CARBOTTE, J. P., 1998, *Phys. Lett. A*, **245**, 172.
- MASON, T. E., SCHRÖDER, A., AEPPLI, G., MOOK, H. A., and HAYDEN, S. M., 1996, *Phys. Rev. Lett.*, **77**, 1604.

- MAXWELL, E., 1950, *Phys. Rev.*, **78**, 477.
- MAZIN, I. I., and YAKOVENKO, V. M., 1995, *Phys. Rev. Lett.*, **75**, 4134.
- MCMAHAN, A. K., MARTIN, R. M., and SATPATHY, S., 1988, *Phys. Rev. B*, **38**, 6650.
- MCQUEENEY, R. J., PETROV, Y., EGAMI, T., YETHIRAJ, M., SHIRANE, G., and ENDOH, Y., 1999, *Phys. Rev. Lett.*, **82**, 628.
- MILLIS, A. J., MONIEN, H., and PINES, D., 1990, *Phys. Rev. B*, **42**, 167.
- MIYAKAWA, N., GUPTASARMA, P., ZASADINSKI, J. F., HINKS, D. G., and GRAY, K. E., 1998, *Phys. Rev. Lett.*, **80**, 157.
- MOOK, H. A., DAI, P. C., HAYDEN, S. M., AEPPLI, G., PERRING, T. G., and DOGAN, F., 1998, *Nature (London)*, **395**, 580.
- MORR, D. K., and PINES, D., 1998, *Phys. Rev. Lett.*, **81**, 1086.
- MORRIS, D. E., SINHA, A. P. B., KIRTIKAR, V., SINGH, K. K., and INYUSHKIN, A. V., 1998, *Physica C* **298**, 203.
- MOURACHKINE, A., 1999, cond-mat/9901282.
- MÜHLSCHLEGEL, B., 1959, *Z. Phys.*, **155**, 313.
- MÜLLER, K. A., 1995, *Nature (London)*, **377**, 133.
- MÜLLER, K. A., ZHAO, G. M., CONDER, K., and KELLER, H., 1998, *J. Phys.: condens. Matter*, **10**, L291.
- MÜLLER, P., ROTHER, S., WALDMANN, O., HEIM, S., MÖSSLE, M., and KLEINER, R., 2000, preprint.
- NAKANO, T., ODA, M., MANABE, C., MOMONO, N., MIURA, Y., and IDO, M., 1994, *Phys. Rev. B*, **49**, 16000.
- NICKEL, J. H., MORRIS, D. E., AGER III, J. W., 1993, *Phys. Rev. Lett.*, **70**, 81.
- NOZAKI, H., and ITOH, S., 1993, *Phys. Rev. B*, **48**, 7583.
- OZYUZER, L., ZASADZINSKI, J. F., KENDZIORA, C., and GRAY, K. E., 2000, *Phys. Rev. B*, **61**, 3629.
- PANAGOPOULOS, C., RAINFORD, B. D., COOPER, J. R., LO, W., TALLON, J. L., LORAM, J. W., BETOURAS, J., WANG, Y. S., and CHU, C. W., 1999, *Phys. Rev. B*, **60**, 14617.
- PELLEGRIN, E., NUCKER, N., FINK, J., MOLODTSOV, S. L., GUTIERREZ, A., NAVAS, E., STREBEL, O., HU, Z., DOMKE, M., KAINDL, G., UCHIDA, S., NAKAMURA, Y., MARKL, J., KLAUDA, M., SAEMANNISCHEN, G., KROL, A., PENG, J. L., LI, Z. Y., and GREENE, R. L., 1993, *Phys. Rev. B*, **47**, 3354.
- PERALI, A., CASTELLANI, C., DI CASTRO, C., GRILLI, M., PIEGARI, E., and VARLAMOV, A. A., 2000, *Phys. Rev. B*, **62**, R9295.
- PETROV, Y., EGAMI, T., MCQUEENEY, R. J., YETHIRAJ, M., MOOK, H. A., and DOGAN, F., 2000, cond-mat/0003414.
- PICKETT, W. E., COHEN, R. E., and KRAKAUER, H., 1991, *Phys. Rev. Lett.*, **67**, 228.
- PINTSCHOVIV, L., and REICHARDT, W., 1994, *Physical Properties of High Temperature Superconductors IV*, edited by D. Ginsberg (Singapore, World Scientific), p. 295.
- PONOMAREV, YA. G., AMINOV, B. A., HEIN, M. A., HEINRICH, H., KRESIN, V. Z., MULLER, G., PIEL, H., ROSNER, K., TCHESNOKOV, S. V., TSOKUR, E. B., WEHLER, D., WINZER, K., YARYGIN, A. V., and YUSUPOV, K. T., 1995, *Physica C*, **243**, 167.
- PROZOROV, R., GIANNETTA, R. W., CARRINGTON, A., FOURNIER, P., GREENE, R. L., GUPTASARMA, P., HINKS, D. G., and BANKS, A. R., 2000a, *Appl. Phys. Lett.*, **77**, 4202.
- PROZOROV, R., GIANNETTA, R. W., FOURNIER, P., and GREENE, R. L., 2000b, *Phys. Rev. Lett.*, **85**, 3700.
- QUIJADA, M. A., TANNER, D. B., KELLEY, R. J., ONELLION, M., BERGER, H., and MARGARITONDO, G., 1999, *Phys. Rev. B*, **60**, 14917.
- RAIMONDI, R., CASTELLANI, C., GRILLI, M., BANG, Y., and KOTLIAR, G., 1993, *Phys. Rev. B*, **47**, 3331.
- RENKER, B., GOMPF, F., GERING, E., EWERT, D., RIETSCHEL, H., and DIANOUX, A., 1988, *Z. Phys. B*, **73**, 309.
- REYNOLDS, C. A., SERIN, B., WRIGHT, W. H., and NESBITT, L. B., 1950, *Phys. Rev.*, **78**, 487.
- SACUTO, A., COMBESCOT, R., BONTEMPS, N., MONOD, P., VIALLET, V., and COLSON, D., 1997, *Europhys. Lett.*, **39**, 207.
- SCHABEL, M. C., PARK, C. H., MATSUURA, A., SHEN, Z. X., BONN, D. A., LIANG, R. X., and HARDY, W. N., 1997, *Phys. Rev. B*, **55**, 2796.
- SCHACHINGER, E., and CARBOTTE, J. P., 2000, *Phys. Rev. B*, **62**, 9054.

- SCHAFROTH, M. R., 1955, *Phys. Rev.*, **100**, 463.
- SCHRIEFFER, J. R., WEN, X. G., and ZHANG, S. C., 1989, *Phys. Rev. B*, **39**, 11 663.
- SHENGLAYLA, A., ZHAO, G. M., AEGERTER, C. M., CONDER, K., SAVIC, I. M., and KELLER, H., 1999, *Phys. Rev. Lett.*, **83**, 5142.
- SHEVCHENKO, P. V., and SUSHKOV, O. P., 1998, *Physica C*, **295**, 292.
- SHOENBERG, D., 1940, *Proc. R. Soc. London, Ser. A*, **175**, 49.
- SMITH, T. J., ANDERSEN, K. H., BECK, U., CAPELLMANN, H., KREMER, R. K., NEUMANN, K. U., SCHARPF, O., SIMON, A., and ZIEBECK, K. R. A., 1998, *J. Magn. magn. Mater.*, **177–181**, 543.
- SONG, Y.-Q., KENNARD, M. A., POEPELMEIER, K. R., and HALPERIN, W. P., 1993, *Phys. Rev. Lett.*, **70**, 3131.
- STADLOBER, B., KRUG, G., NEMETSCHKE, R., HACKL, R., COBB, J. L., and MARKERT, J. T., 1995, *Phys. Rev. Lett.*, **74**, 4911.
- STERNLIEB, B. J., LUKE, G. M., UEMURA, Y. J., RISEMAN, T. M., BREWER, J. H., GEHRING, P. M., YAMADA, K., HIDAKA, Y., MURAKAMI, T., THURSTON, T. R., and BIRGENEAU, R. J., 1990, *Phys. Rev. B*, **41**, 8866.
- SUN, A. G., GAJEWSKI, D. A., MAPLE, M. B., and DYNES, R. C., 1994, *Phys. Rev. Lett.*, **72**, 2267.
- SUZUKI, K., ICHIMURA, K., NOMURA, K., and TAKEKAWA, S., 1999a, *Phys. Rev. Lett.*, **83**, 616.
- SUZUKI, M., WATANABE, T., and MATSUDA, A., 1999b, *Phys. Rev. Lett.*, **82**, 3302.
- TAMASAKU, K., ITO, T., TAKAGI, H., and UCHIDA, S., 1994, *Phys. Rev. Lett.*, **72**, 3088.
- THELEN, D., PINES, D., and LIU, J. P., 1993, *Phys. Rev. B*, **47**, 9151.
- THIO, T., THURSTON, T. R., PREYER, N. W., PICONE, P. J., KASTNER, M. A., JENSSEN, H. P., GABBE, D. R., CHEN, C. Y., BIRGENEAU, R. J., and AHARONY, A., 1988, *Phys. Rev. B*, **38**, 905.
- TRANQUADA, J. M., STERNLIEB, B. J., AXE, J. D., NAKAMURA, Y., and UCHIDA, S., 1995, *Nature (London)*, **375**, 561.
- TSUEI, C. C., and KIRTLEY, J. R., 2000, *Phys. Rev. Lett.*, **85**, 182.
- TSUEI, C. C., KIRTLEY, J. R., RUPP, M., SUN, J. Z., GUPTA, A., KETCHEN, M. B., WANG, C. A., REN, Z. F., WANG, J. H., and BHUSHAN, M., 1996, *Science*, **271**, 329.
- TSUEI, C. C., KIRTLEY, J. R., RUPP, M., SUN, J. Z., YUJAHNES, L. S., CHI, C. C., GUPTA, A., and KETCHEN, M. B., 1995, *J. Phys. Chem. Solids*, **56**, 1787.
- UCHIDA, S., 1997, *Physica C*, **282–287**, 12.
- UEMURA, Y. J., LUKE, G. M., STERNLIEB, B. J., BREWER, J. H., CAROLAN, J. F., HARDY, W. N., KADONO, R., KEMPTON, J. R., KIEFL, R. F., KREITZMAN, S. R., MULHERN, P., RISEMAN, T. M., WILLIAMS, D. L., YANG, B. X., UCHIDA, S., TAKAGI, H., GOPALAKRISHNAN, J., SLEIGHT, A. W., SUBRAMANIAN, M. A., CHIEN, C. L., CIEPLAK, M. Z., XIAO, G., LEE, V. Y., STATT, B. W., STRONACH, C. E., KOSSLER, W. J., and YU, X. H., 1989, *Phys. Rev. Lett.*, **62**, 2317.
- VOBORNIK, I., GATT, R., SCHMAUDER, T., FRAZER, B., KELLEY, R. J., KENDZIORA, C., GRIONI, M., ONELLION, M., and MARGARITONDO, G., 1999, *Physica C*, **317–318**, 589.
- WEI, J. Y. T., YEH, N.-C., GARRIGUS, D. F., and STRASIK, M., 1998, *Phys. Rev. Lett.*, **81**, 2542.
- WERMBTER, S., and TEWORDT, L., 1992, *Phys. Rev. B*, **46**, 12061.
- WHITE, P. J., SHEN, Z. X., KIM, C., HARRIS, J. M., LOESER, A. G., FOURNIER, P., and KAPITULNIK, A., 1996, *Phys. Rev. B*, **54**, 15 669.
- WILLEMEN, M., ROSSEL, C., BRUGGER, J., DESPONT, M. H., ROTHUIZEN, H., VETTIGER, P., HOFER, J., KELLER, H., 1998a, *J. Appl. Phys.*, **83**, 1163.
- WILLEMEN, M., ROSSEL, C., HOFER, J., KELLER, H., REN, Z. F., and WANG, J. H., 1998b, *Phys. Rev. B*, **57**, 6137.
- WILLEMEN, M., ROSSEL, C., HOFER, J., KELLER, H., and REVCOLEVSKI, A., 1999, *Phys. Rev. B*, **59**, R717.
- WILLEMEN, M., SCHILLING, A., KELLER, H., ROSSEL, C., HOFER, J., WELP, U., KWOK, W. K., OLSSON, R. J., and CRABTREE, G. W., 1998c, *Phys. Rev. Lett.*, **81**, 4236.
- WILLIAMS, G. V. M., PRINGLE, D. J., and TALLON, J. L., 2000, *Phys. Rev. B*, **61**, R9257.
- WU, D. H., MAO, J., MAO, S. N., PENG, J. L., XI, X. X., VENKATESAN, T., GREENE, R. L., and ANLAGE, S. M., 1993, *Phys. Rev. Lett.*, **70**, 85.

- YAGIL, Y., HASS, N., DESGARDIN, G., and MONOT, I., 1995, *Physica C*, **250**, 59.
- YIN, L., CHAKRAVARTY, S., and ANDERSON, P. W., 1997 *Phys. Rev. Lett.*, **78**, 3559.
- ZECH, D., KELLER, H., CONDER, K., KALDIS, E., LIAROKAPIS, E., POULAKIS, N., and MÜLLER, K. A., 1994, *Nature (London)*, **371**, 681.
- ZHAO, G. M., AGER III, J. W., and MORRIS, D. E., 1996a, *Phys. Rev. B*, **54**, 14982.
- ZHAO, G. M., CONDER, K., ANGST, M., KAZAKOV, S. M., KARPINSKI, J., MACIEJEWSKI, M., BOUGEROL, C., PSHIRKOV, J. S., and ANTIPOV, E. V., 2000a, *Phys. Rev. B*, **62**, R11977.
- ZHAO, G. M., CONDER, K., KELLER, H., and MÜLLER, K. A., 1996b, *Nature (London)*, **381**, 676; 1998a, *J. Phys.: condens. Matter*, **10**, 9055.
- ZHAO, G. M., GHOSH, K., and GREENE, R. L., 1998b, *J. Phys.: condens. Matter*, **10**, L737.
- ZHAO, G. M., GHOSH, K., KELLER, H., and GREENE, R. L., 1999, *Phys. Rev. B*, **59**, 81.
- ZHAO, G. M., HUNT, M. B., KELLER, H., and MÜLLER, K. A., 1997, *Nature (London)*, **385**, 236.
- ZHAO, G. M., KIRTIKAR, V., SINGH, K. K., SINHA, A. P. B., MORRIS, D. E., INYUSHKIN, A. V., 1996c, *Phys. Rev. B*, **54**, 14956.
- ZHAO, G. M., and MORRIS, D. E., 1995, *Phys. Rev. B*, **51**, 16487.
- ZHAO, G. M., SINGH, K. K., and MORRIS, D. E., 1994, *Phys. Rev. B*, **50**, 4112.
- ZHAO, G. M., SINGH, K. K., SINHA, A. P. B., MORRIS, D. E., 1995, *Phys. Rev. B*, **52**, 6840.
- ZHAO, G. M., WANG, Y. S., KANG, D. J., PRELLIER, W., RAJESWARI, M., KELLER, H., VENKATESAN, T., and CHU, C. W., 2000b, *Phys. Rev. B*, **62**, R11949.
- ZUTIC, I., and VALLS, O. T., 1997, *Phys. Rev. B*, **56**, 11279.